NEUROSCIENCE

Experience-dependent plasticity of gustatory insular cortex circuits and taste preferences

Hillary C. Schiff[1], Joshua F. Kogan[1,2,3], Maria Isaac[1,2], Lindsey A. Czarnecki[1], Alfredo Fontanini[1,2], Arianna Maffei[1,2]*

Early experience with food influences taste preference in adulthood. How gustatory experience influences development of taste preferences and refinement of cortical circuits has not been investigated. Here, we exposed weanling mice to an array of taste solutions and determined the effects on the preference for sweet in adulthood. We demonstrate an experience-dependent shift in sucrose preference persisting several weeks following the termination of exposure. A shift in sucrose palatability, altered neural responsiveness to sucrose, and inhibitory synaptic plasticity in the gustatory portion of the insular cortex (GC) were also induced. The modulation of sweet preference occurred within a restricted developmental window, but restoration of the capacity for inhibitory plasticity in adult GC reactivated the sensitivity of sucrose preference to taste experience. Our results establish a fundamental link between gustatory experience, sweet preference, inhibitory plasticity, and cortical circuit function and highlight the importance of early life nutrition in setting taste preferences.

INTRODUCTION

Taste preferences guide food choices, thereby affecting health and quality of life. At the transition from relying on mother's milk to foraging, animals learn to independently taste food and act upon it, approaching and consuming nourishing food or avoiding and rejecting dangerous substances. In animals, preferences for key tastes such as sweet are viewed as innate (*1*), yet they can be influenced by early life experience (*2*, *3*). Even in human infants, early taste experiences modulate gustatory preferences later in life (*2*, *4*).

In adults, the gustatory portion of the insular cortex, the gustatory cortex (GC), plays a central role in a variety of taste-related functions, including integrating information about identity and hedonic value of taste (*5*, *6*), predicting the occurrence of a taste based on food's anticipatory cues (*7*–*10*), learning about safety or danger related to tastes (*11*, *12*), forming associations between tastes and postingestive effects (*13*), and making taste-informed decisions (*14*, *15*). These findings highlight GC plasticity and point to the possibility that circuits in GC may be sensitive to experience with taste. While the role of experience in shaping preferences has been demonstrated in adult flies (*16*), there is no information about the relationship of taste experience during postnatal development, taste preference, and neural circuit function in gustatory cortical circuits.

Here, we investigated whether taste experience at weaning modulates the preference for sweet later in life and assessed the neural underpinnings of taste exposure in mouse GC. We report that early life exposure to tastes has profound and persistent effects on sweet preference, neural responses to sucrose, and the postnatal maturation of inhibitory circuits in GC. The same exposure started in adulthood did not affect sucrose preference, indicating the presence of a sensitive period for the experience-dependent modulation of sweet preference. Manipulation of GC inhibition in adult mice was sufficient to reopen the sensitive window and restore taste-dependent plasticity in adult mice. To our knowledge, this is the first study to directly link early life dietary experience with cortical circuit plasticity and responsiveness to tastants in adulthood, indicating a powerful effect of the integration of chemosensory experience and nutrition on brain development.

[1]Department of Neurobiology and Behavior, SUNY Stony Brook, Stony Brook, NY, USA. [2]Graduate Program in Neuroscience, SUNY Stony Brook, Stony Brook, NY, USA. [3]Medical Scientist Training Program, SUNY Stony Brook, Stony Brook, NY, USA. *Corresponding author. Email: arianna.maffei@stonybrook.edu

RESULTS

Taste exposure early in life enhanced the preference for sucrose

We developed a taste exposure paradigm to manipulate taste experience (Fig. 1). Weanlings were given repeated access to four different solutions ["early exposure" (EE); Fig. 1A] in their home cage drinking bottle on an 8-day schedule [Fig. 1A and Table 1; 150 mM sucrose (S) on days 1 and 5, 20 mM citric acid (CA) on days 2 and 6, Ensure (E) on days 3 and 7, and 100 mM salt (NaCl) on days 4 and 8]. Following exposure, EE mice returned to a diet of chow and water until the end of the experiment. A separate group of littermates was assigned to the control group ("naïve") and maintained on a standard diet of chow and water. In separate sets of

Table 1. Training schedule for the BAT.

Day	Training (all sessions 30 min)	Access to water
1	Context habituation	Water bottle removed after training session
2	Spout training	Only during training
3	Shutter training	10 min at the end of the day
4	Collection first sucrose curve	5 min with water 2 hours before testing and 10 min at the end of sucrose curve collection
5	Collection second sucrose curve	5 min with water 2 hours before testing; returned to ad libitum food and water at the end of sucrose curve collection

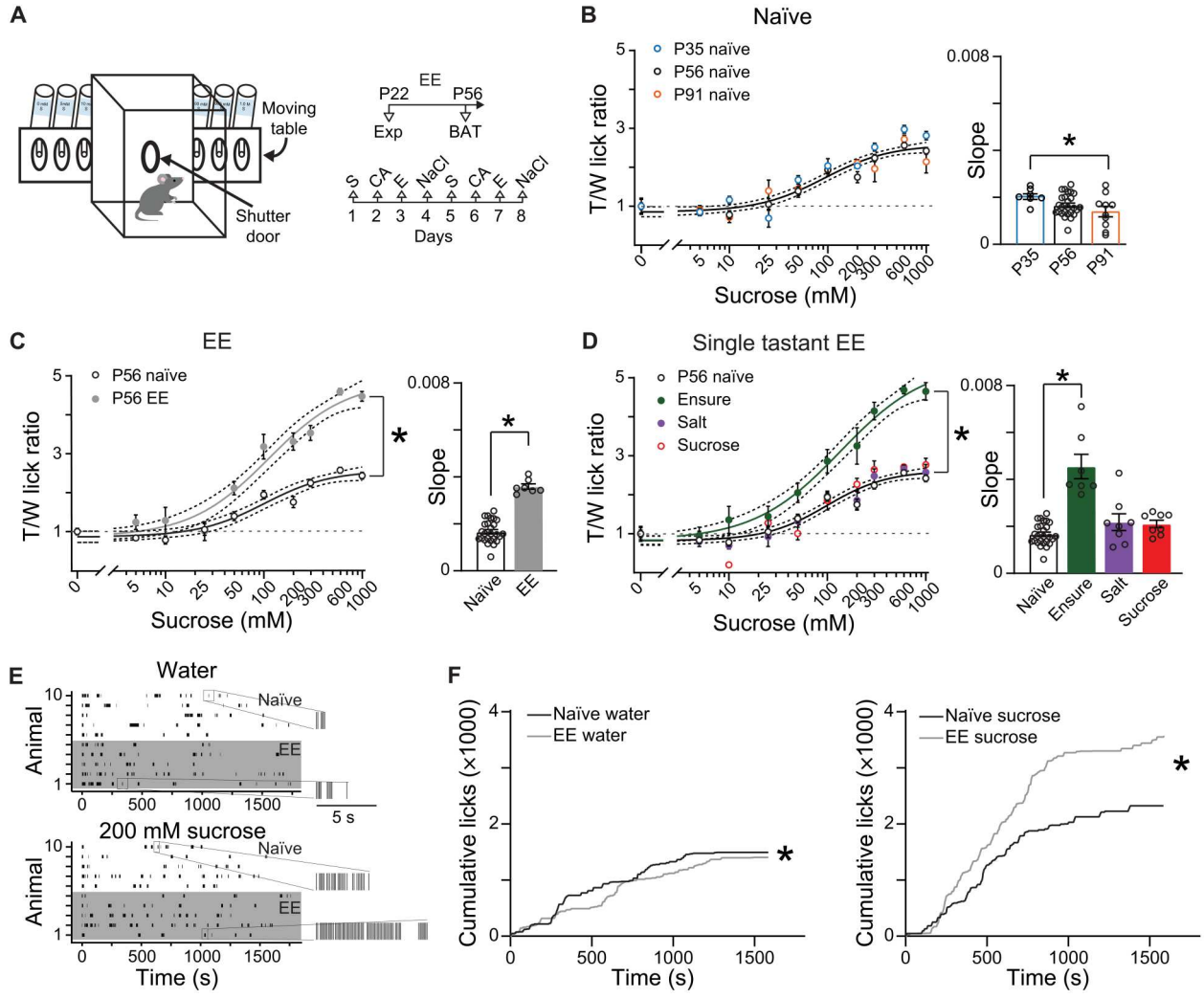

Fig. 1. Early exposure (EE) induced long-lasting changes in sucrose preference. (**A**) Left: Representation of Davis rig gustometer. Top right: Schedule for EE and testing. Bottom right: Sequence of taste solutions. (**B**) Left: Sucrose curves from naïve mice by age group. A single curve fitted all datasets (P = 0.071, F test). Right: Slopes of sucrose curves for naïve mice (P = 0.040, one-way analysis of variance (ANOVA); P35 versus P91, P = 0.035, post hoc Bonferroni test). (**C**) Left: Sucrose curve for P56 naïve (black) and EE (gray) mice. Separate curves were needed to fit the datasets (P < 0.001, F test). Right: Slope of P56 naïve (white) and EE (gray) sucrose curves ($P = 1.831 \times 10^{-11}$, unpaired two-tailed t test). (**D**) Left: Sucrose curves for P56 mice in modified EE. Separate curves were needed for Ensure (P < 0.001, F test), while a single curve was sufficient to fit naïve (black), NaCl (purple), and sucrose (red) (P = 0.115, F test). Right: Slope of sucrose curves. White, naïve; green, Ensure EE; purple, NaCl EE; red, sucrose EE (naïve versus Ensure, $P = 4.69 \times 10^{-11}$; naïve versus sucrose, P = 0.423; naïve versus salt, P = 0.290; one-way ANOVA with post hoc Bonferroni t test). For (B) to (D), dark line, curve fit; dotted lines, 95% CIs. Dotted gray line plotted at 1 shows water lick rate (0 mM sucrose). Data points, means ± SEM. (**E** and **F**) Analysis of licking for P55 to P58 naïve and EE mice tested on a 30-min trial of access to water or 200 mM sucrose. (E) Lick raster plots for water (top) and sucrose (bottom). Shaded area, licks by mice in the EE group. (F) Left: Accumulation of licks to water from naïve (black) and EE (gray) mice ($P = 8.2 \times 10^{-10}$, Mann-Whitney U test). Right: Accumulation of licks to sucrose in naïve (black) and EE (gray) mice ($P = 5.2 \times 10^{-5}$, Mann-Whitney U test). Asterisks indicate $P \leq 0.05$.

control experiments, a group of naïve mice was used to confirm that all solutions were consumed comparably or more than water. Sucrose and Ensure were preferred over water, consistent with an innate preference for sweet taste, while NaCl and citric acid were consumed comparably to water (fig. S1A). We also verified that there was no difference in body weight between mice in the naïve and EE groups during or after EE (fig. S1B).

We used a brief access test (BAT) to determine the effects of EE on sweet preference. Preference was assessed by measuring licking to different concentrations of sucrose with a Davis rig gustometer (Fig. 1A) (*17*) and quantifying the tastant-to-water (T/W) lick ratio for each stimulus concentration. BAT exposes mice to different concentrations of sucrose (0, 5, 10, 25, 50, 100, 200, 300, 600, and 1000 mM) for multiple, brief (10-s) trials. There were no developmental changes in sucrose preference curve in distinct cohorts of naïve mice from three distinct age groups [Fig. 1B; postnatal day 35 (P35), n = 7 mice; P56, n = 26 mice; and P91, n = 10 mice; $F_{(6,420)}$ = 1.956, P = 0.071, F test]. The slope of the curves showed a small, but significant decrease between P35 and P91 [slopes: $F_{(2,40)}$ = 3.50, P = 0.040, one-way analysis of variance (ANOVA) with post hoc Bonferroni corrected t tests: P35 versus P56, P = 0.235; P35 versus P91, P = 0.035; and P56 versus P91, P = 0.476], suggesting

that sucrose preference is overall stable in mice maintained on their regular diet, as previously shown (*18*). In contrast, sucrose preference was enhanced in mice from the EE group when assessed either at P35 (fig. S1C), P56 (Fig. 1C), and 1 or 4 weeks from the end of EE, respectively. The shift in preference was detectable also in a group of mice tested at P70 (fig. S1D), indicating that 8 days of exposure at P21 could modulate sweet preference for at least 6 weeks after the end of the EE paradigm. Separate sigmoid functions were required to fit the datasets from age-matched naïve and EE mice, and the slope of the sucrose preference curves were significantly different [Fig. 1C; P56: sucrose curve: naïve, n = 26 mice; EE, n = 7 mice; $F_{(3,323)}$ = 79.76, P < 0.0001, F test; P56 slope: $t_{(31)}$ = 10.24, P < 0.0001, two-tailed unpaired t test]. Unless otherwise stated, our analysis of preference focused on P56. For each experimental condition, a group of naïve and one of EE littermates were run in parallel.

The observed shift in sucrose preference did not depend on familiarity with sucrose, as 8 days of exposure to sucrose alone did not shift the preference curve measured at P56 (Fig. 1D), in line with previous observations (*19*). Experience with salt may also influence sweet preference (*20*), but 8 days of exposure to NaCl alone did not affect the sucrose curve [Fig. 1D; naïve, n = 26 mice; sucrose EE, n = 7 mice; salt EE, n = 8 mice; $F_{(6,399)}$ = 1.720, P = 0.115, F test]. However, 8 days of Ensure induced a shift comparable to that observed with the EE paradigm [Fig. 1D; naïve, n = 26 mice; Ensure EE, n = 7 mice; $F_{(3,318)}$ = 83.06, P < 0.0001, F test]. The slope of the sucrose preference curves from the Ensure EE group was also significantly different from naïve, while sucrose EE and salt EE were not [Fig. 1D; naïve, n = 26 mice; sucrose EE, n = 7 mice; salt EE, n = 8 mice; Ensure EE, n = 7 mice; $F_{(3,44)}$ = 27.07, P = 4.473 × 10^{-10}, one-way ANOVA with post hoc Bonferroni t tests; naïve versus sucrose, P = 0.423; naïve versus salt, P = 0.290; naïve versus Ensure, P = 4.69 × 10^{-11}].

To determine whether the shift in sucrose curve represents increased palatability for this tastant, we analyzed licking microstructure, a widely used approach to assess different aspects of taste perception (*21*). We compared licking behavior in naïve and EE mice, which had access to water or 200 mM sucrose for a 30-min trial on subsequent days (Fig. 1E and fig. S2A). The number of bouts of licks for water and sucrose was comparable (fig. S2B), but in EE mice, bout size (measured as licks per bout) for sucrose was significantly larger (fig. S2C). Last, mice in the EE group accumulated licks for water more slowly than naïve mice (Fig. 1F, left), while they accumulated licks more rapidly for sucrose (Fig. 1F, right; left, water: naïve, n = 1496 licks; EE, n = 1405 licks; U = 927,887, P = 8.2 × 10^{-10}; right, sucrose: naïve, n = 2324 licks; EE, n = 3583 licks; U = 3,872,876, P = 5.2 × 10^{-5}; Mann-Whitney U test). As bout size is directly linked to palatability (*22*) and accumulation of licks is evidence of increased avidity to sucrose (*23*), these results indicate that mice in the EE group perceived sucrose as more palatable than naïve mice.

To assess whether the shift in the sucrose curve represents shift in preference specific to sucrose or it extends to other tastants, we compared the curve for saccharin and salt obtained from separate groups of naïve and EE mice. The preference for saccharin was significantly increased in mice from the EE group (fig. S3A), while it did not affect the preference for salt (fig. S3B). These results suggest that experience-dependent changes in sucrose preference generalize to other sweet tastes but do not extend to salt.

Integration of taste, olfaction, and postingestive components modulated sweet preference

The shift in sucrose preference observed in the EE paradigm and in the Ensure EE (Fig. 1, C and D) could have resulted from a variety of factors, including exposure to tastants and nutrients, postingestive effects due to caloriecontent, and/or the olfactory component of Ensure. To begin testing the role of postingestive effects, we ran a calorie-free version of EE, in which sucrose was replaced with saccharin, and Ensure was replaced with monosodium glutamate (MSG). This paradigm preserves the oral sensation of taste and the variety of taste qualities (sweet, sour, salt, and umami) but does not engage postingestive mechanisms. The calorie-free exposure did not shift the sucrose preference curve or the slope of the curve [Fig. 2A; left, sucrose curve: naïve, n = 26 mice; calorie-free EE, n = 9 mice; $F_{(3,343)}$ = 0.7430, P = 0.527, F test; right, slope: $t_{(58)}$ = 0.458, P > 0.999, Bonferroni-corrected t test], indicating that calories play a role in the experience-dependent modulation of sucrose preference. To further assess the importance of the postingestive contributions, we tested a cohort of mice which received 8 days of Ensure by tube feeding beginning on P22. The control group was tube-fed with water. This version of EE exposed mice to calories and engaged postingestive mechanisms in the absence of the oral sensation of taste. Intragastric exposure to Ensure did not affect the sucrose preference curve (Fig. 2B) or its slope [Fig. 2B; left, sucrose curve: water, n = 5 mice; Ensure, n = 7 mice; $F_{(3,113)}$ = 1.936, P = 0.128, F test; right, slope: $t_{(10)}$ = 0.8322, P = 0.425, unpaired two-tailed t test]. These results point at integration of orosensory and enteric information in the experience-dependent modulation of sweet preference.

To assess the possible contribution of the olfactory component of Ensure, we induced temporary anosmia during EE (*24*). Mice received an intranasal instillation of either saline (control group) or $ZnSO_4$ (temporary anosmia group) before receiving Ensure EE. This manipulation did not affect the amount of Ensure consumed (fig. S4A) or body weight (fig. S4B). We verified anosmia and recovery of smell in a separate group of mice (fig. S4, C to E). Mice rendered temporarily anosmic during Ensure EE showed a reduction in the sucrose preference curve compared to intact Ensure-EE mice. This shift was accompanied by a decrease in the slope of the preference curve [Fig. 2C; left, sucrose curve: saline, n = 9; $ZnSO_4$, n = 8; $F_{(3,163)}$ = 19.65, P = 6.349 × 10^{-11}, F test; right, slope: saline, $t_{(15)}$ = 3.420; P = 0.0038, two-tailed unpaired t test], indicating that the olfactory component of Ensure contributed to the experience-dependent enhancement in sucrose preference. Together, the results of these assays support the conclusion that early experience with taste solutions persistently increase sucrose preference and palatability and that the modulation of sucrose preference depends on the integration of sensory (gustatory and olfactory) and postingestive components.

Taste exposure early in life modulated neural responses to sucrose

Motivated by its role in taste processing and taste guided behaviors (*15*, *25*, *26*), we focused on the GC as a possible circuit regulating taste preferences. We used two-photon calcium imaging in awake naïve and EE mice to measure baseline activity and sucrose-evoked responses of GC neurons during active licking for various concentrations (Fig. 3, A and B; 0, 25, 50, 100, 200, and 600 mM). We used the offspring of *PV-cre* (*27*) and *floxed-tdTomato* mice (*28*)

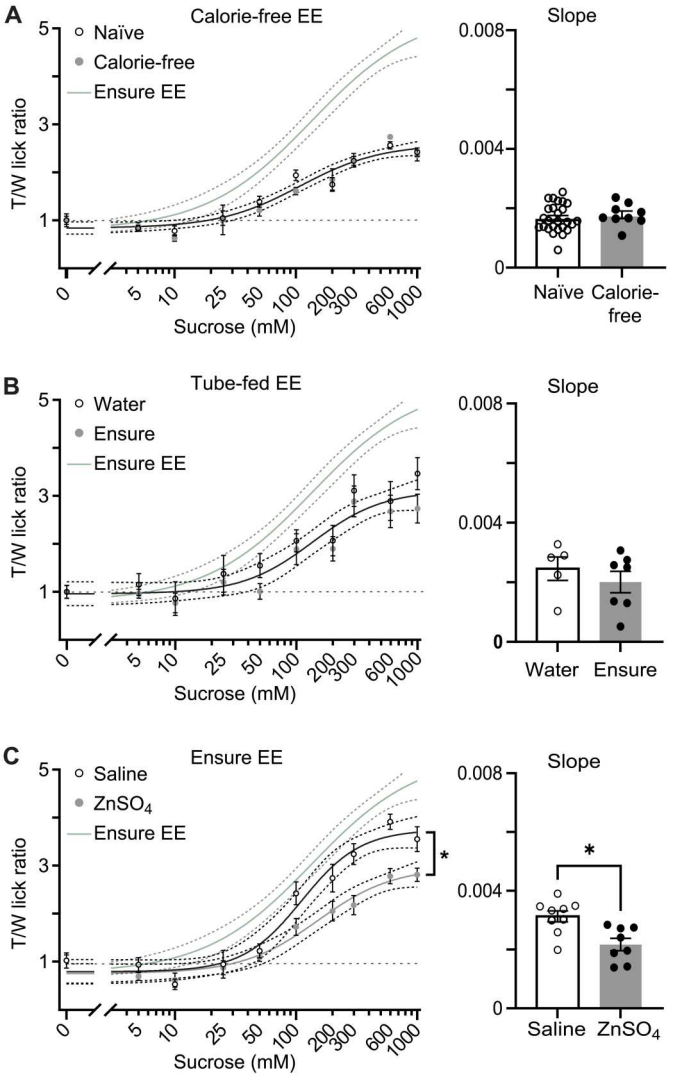

Fig. 2. The effect of EE depended on integration of orosensory, postingestive, and olfactory activity. (**A**) Sucrose curve for P56 naïve (black) and calorie-free EE (gray) mice. A single curve was sufficient to fit both datasets ($P = 0.527$, F test), and the slope of the curves did not differ ($P > 0.999$, t test with Bonferroni correction for multiple comparisons). (**B**) Sucrose curve for P56 mice tube-fed with water (black) or with Ensure (gray) from P22 to P29. A single curve was sufficient to fit both datasets ($P = 0.128$, F test), and the slope of the curves did not differ ($P = 0.425$, t test). (**C**) Sucrose curve for P56 mice with Ensure EE treated with either saline or $ZnSO_4$ at P21. Separate curves were needed to fit the datasets ($P = 6.349 \times 10^{-11}$, F test), and the slope of the preference curve were significantly different ($P = 0.0038$, t test). Note that the sucrose curve and the slope of the curve in $ZnSO_4$ mice indicate decreased preference. To facilitate visual comparison with the sucrose curve for Ensure EE, the fit of the sucrose curve for Ensure EE from Fig. 1D was added to the plots in (A), (B), and (C) (Ensure EE, light gray). Asterisks indicate $P \leq 0.05$.

(Fig. 3, A and C) to record calcium signals simultaneously from pyramidal (PYR) and parvalbumin-positive (PV^+) neurons. We extracted $\Delta F/f$ traces and deconvolved activity using a widely adopted algorithm (see Materials and Methods; Fig. 3, D and E) (*29*). We focused on PV^+ γ-aminobutyric acid (GABA)–releasing (GABAergic) neurons because they are highly sensitive to changes in postnatal sensory experience in other cortices (*30*, *31*) and influence taste-based memory formation in GC (*32*). We recorded 5224 neurons over 12 sessions from five mice for the naïve group (4994 PV^- putative PYR; 230 PV^+ neurons) and 4795 neurons in 15 sessions from five mice for the EE group (4573 PYR; 222 PV^+ neurons). Neural activity was monitored during the baseline period of the trial (Fig. 3, F and G, 2-s window before trial onset; and fig. S5, 4-s window before trial onset. Note that comparable results were obtained in short and long baseline windows). Following EE, this baseline activity was reduced in PYR neurons [Fig. 3, F and G, top; naïve, $n = 4994$ neurons; EE, $n = 4573$ neurons; $P = 0.013$, Kolmogorov-Smirnov (K-S) test; see also fig. S5, A and B, top], while it was increased in PV^+ neurons (Fig. 3, F and G, bottom; naïve, $n = 230$ neurons; EE, $n = 222$ neurons; $P = 7.92 \times 10^{-9}$, K-S test; see also fig. S5, A and B, bottom), suggesting that the GC circuit leans toward higher inhibition in EE mice. In addition, fewer PYR neurons were activated by sucrose [Fig. 3H; naïve, $n = 729$ of 4994 (14.6%); EE, $n = 387$ of 4573 (8.5%); $\chi2(1) = 87.19$, $P < 0.0001$, χ^2 test], while the number of PV^+ neurons responsive to sucrose was unchanged (Fig. 3H; naïve, $n = 18$ of 230 (7.8%), versus EE, $n = 20$ of 222 (9%); $\chi2(1) = 0.2053$, $P = 0.69$, chi-square test). Thus, following EE, the ratio of sucrose-activated excitatory to inhibitory neurons in GC was reduced. GC activity can be modulated by licking. Thus, to determine whether the shift in activity may be related to a change in lick frequency during taste sampling, we measured this parameter in the 1.5-s window in which the spout was available to the mice. As shown in fig. S6A, EE did not affect lick frequency in this brief time window. This lack of difference is consistent with what observed over the 10-s window of sipper tube availability during the BAT (fig. S6B). These results indicate that differences in GC neural activity between naïve and EE mice are not driven by altered lick frequency over the short time of availability of the tastant in two-photon imaging experiments. Rather, differences in lick patterns emerged only over long periods of time when mice had the opportunity to consume the taste in multiple bouts (30 min, as in Fig. 1, E and F, and fig. S2C).

To investigate whether the reduced activation of putative PYR neurons modulated their responsiveness to sucrose concentrations, we fitted average responses to each concentration with a linear function and calculated the slope and 95% confidence interval (CI) of the linear fit (see Materials and Methods; Fig. 3, I and J). There was an increased proportion of neurons with a significant fit in the EE group compared with naïve, and this effect was specific to the sampling window [Fig. 3K; baseline: naïve, $n = 123$ of 729 (16.9%); EE, $n = 68$ of 387 (17.6%); $\chi2(1) = 0.087$, $P = 0.77$; sampling: naïve, $n = 123$ of 729 (16.9%); EE, $n = 101$ of 387 (26.0%); $\chi2(1) = 13.41$, $P < 0.001$, chi-square test]. There was also a significant increase in the absolute slope of the fits [Fig. 3L; baseline: $t_{(1)} = 0.096$, $P = 0.92$; sampling: $t_{(1)} = 2.16$, $P < 0.05$, unpaired two-tailed t test]. Thus, following EE, the spontaneous activity of PYR neurons decreased, while that of PV^+ neurons increased, shifting the excitation/inhibition (E/I) balance of the GC network. Consistent with a decreased E/I ratio, fewer PYR neurons responded to sucrose. However, the ones that did respond were more sensitive to sucrose concentrations, indicating that EE had persistent effects on GC circuit excitability, circuit responsiveness, and coding for sucrose concentrations.

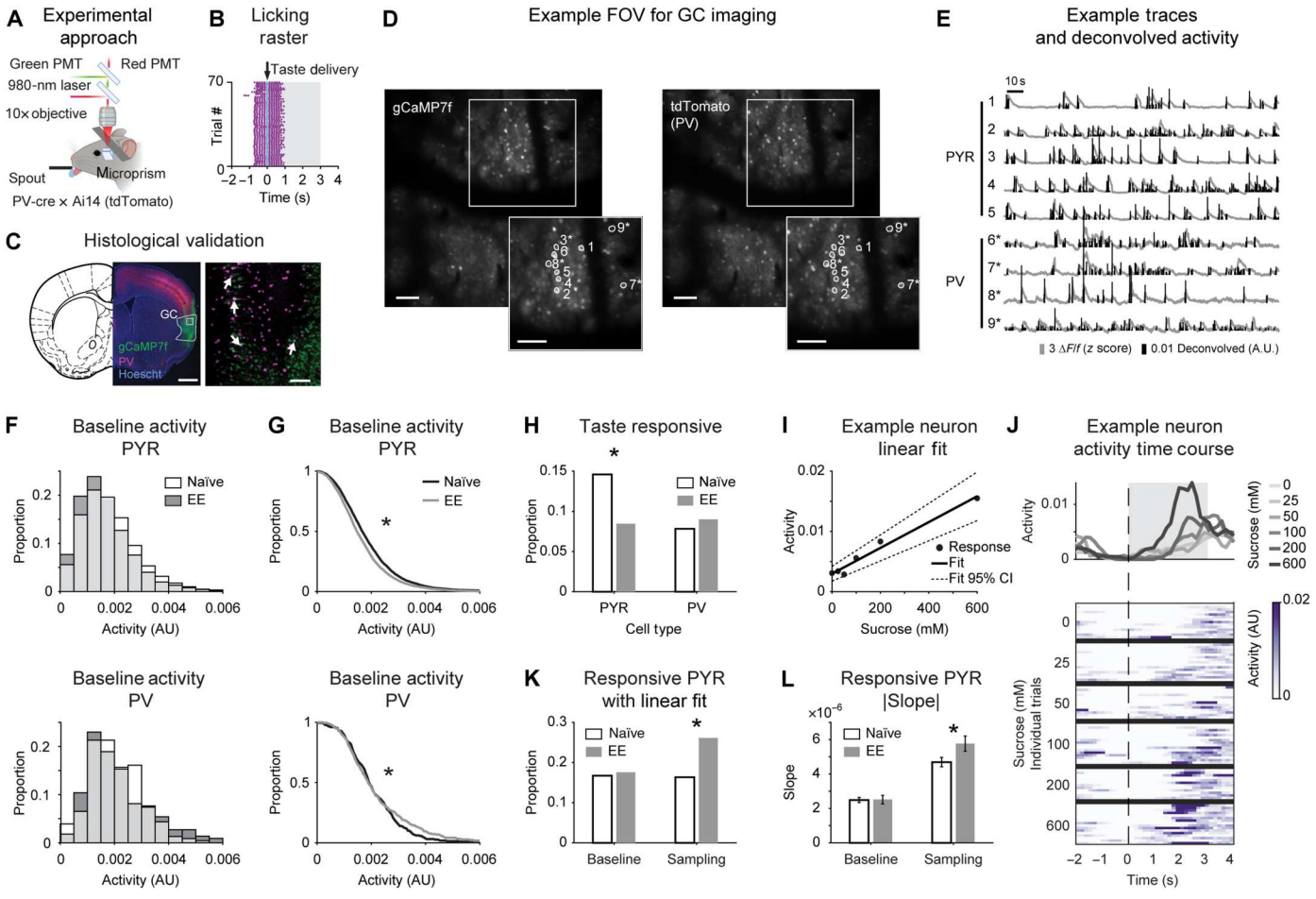

Fig. 3. EE modulates GC neural responses. (**A**) Experimental approach for imaging in GC. (**B**) Representative lick raster of trial structure. Shading, response window. (**C**) Left: Representative coronal section of gCaMP7f expression, PV$^+$ neurons, and Hoechst 33342; scale bar, 1 mm. Right: High magnification of inset. Arrows, PV$^+$ neurons with gCaMP7f; scale bar, 100 μm. (**D**) Representative two-photon field of view (FOV) for gCaMP7f (left) and tdTomato (right); scale bars, 100 μm. Insets: ROIs for nine example neurons (* = tdTomato$^+$); scale bars, 100 μm. (**E**) Example traces of $\Delta F/f$ and deconvolved activity for PYR and PV$^+$ neurons in (D). (**F**) Distribution of baseline activity for all PYR (top: naïve, $n = 4994$; EE, $n = 4573$) and PV$^+$ (bottom: naïve, $n = 230$; EE, $n = 222$) neurons. Naïve, white; EE, dark gray; light gray, overlap for naïve and EE. (**G**) Cumulative distribution of baseline activity for all PYR (top: $P = 0.013$, K-S test) and PV$^+$ neurons (bottom: $P = 7.92 \times 10^{-9}$, K-S test). (**H**) Proportion of taste responsive PYR (white bar: naïve, 729 of 4994; gray bar: EE, 387 of 4573) and PV$^+$ neurons (white bar: naïve, 18 of 230; gray bar: EE, 20 of 222; PYR, $P < 0.0001$; PV$^+$, $P = 0.65$, $\chi 2$ test). (**I**) Representative neuron with significant linear fit to sucrose responses. Black circles, response to each sucrose concentration; black line, linear fit; dashed lines, 95% CI. (**J**) Activity from neuron in (I). Dashed line, taste delivery. Top: Peristimulus time histogram of responses to sucrose concentrations. Bottom: Heatmap of individual trial responses sorted by concentration (96 trials total). (**K**) Proportion of PYR neurons with significant linear fits at baseline (white bar: naïve, 123 of 729; gray bar: EE, 68 of 387; $P = 0.77$, $\chi 2$ test) and sampling (white bar: naïve, 123 of 729; gray bar: EE, 101 of 387; $P < 0.001$, $\chi 2$ test) windows. (**L**) Absolute slope of PYR neurons with significant linear fit [same neurons as (K); baseline, $P = 0.92$; sampling, $P < 0.05$, unpaired t test]. Asterisks indicate $P \leq 0.05$. AU, arbitrary units.

Taste experience early in life enhanced inhibitory synaptic transmission in GC

Reduced spontaneous activity, response suppression in PYR neurons, and increased spontaneous activity of PV$^+$ neurons may be due to reduced excitability of PYR neurons, increased excitability of PV$^+$ neurons, or changes in synaptic transmission. To test these possibilities, we used patch clamp recordings from acute slice preparations obtained from naïve and EE mice at P56 (Fig. 4 and fig. S7). For these experiments, as for the imaging in vivo, we used the offspring of *PV-cre* (*27*) and *floxed-tdTomato* mice (*28*) to visualize PV$^+$ and PV$^-$ neurons and record from both PV$^+$ and PYR populations. Recorded neurons were filled with biocytin for post hoc reconstruction of morphology, location, and immunohistochemistry. We confirmed the GABAergic nature of recorded PV$^+$ neurons and the excitatory nature of PYR neurons using post hoc immunohistochemistry for glutamic acid decarboxylase 67 (GAD67) (Fig. 4A and fig. S7, A and E). We obtained input/output functions by injecting square current pulses of increasing amplitudes and quantifying the frequency of action potentials (APs) (fig. S7, B, C, F, and G). Naïve and EE mice showed no differences in either PYR or PV$^+$ neurons input/output curves (fig. S7, C and G), input resistance, rheobase, and AP threshold (fig. S7, D and H). Thus, EE did not modulate the intrinsic excitability in either PYR or PV$^+$ neurons.

To test the possibility that EE modulates synaptic transmission onto GC PYR neurons, voltage clamp recordings were obtained from confirmed PYR neurons in acute slice preparations of P56 naïve and EE wild-type mice (Fig. 4A and fig. S8). Spontaneous excitatory and inhibitory postsynaptic currents (sEPSCs and sIPSCs,

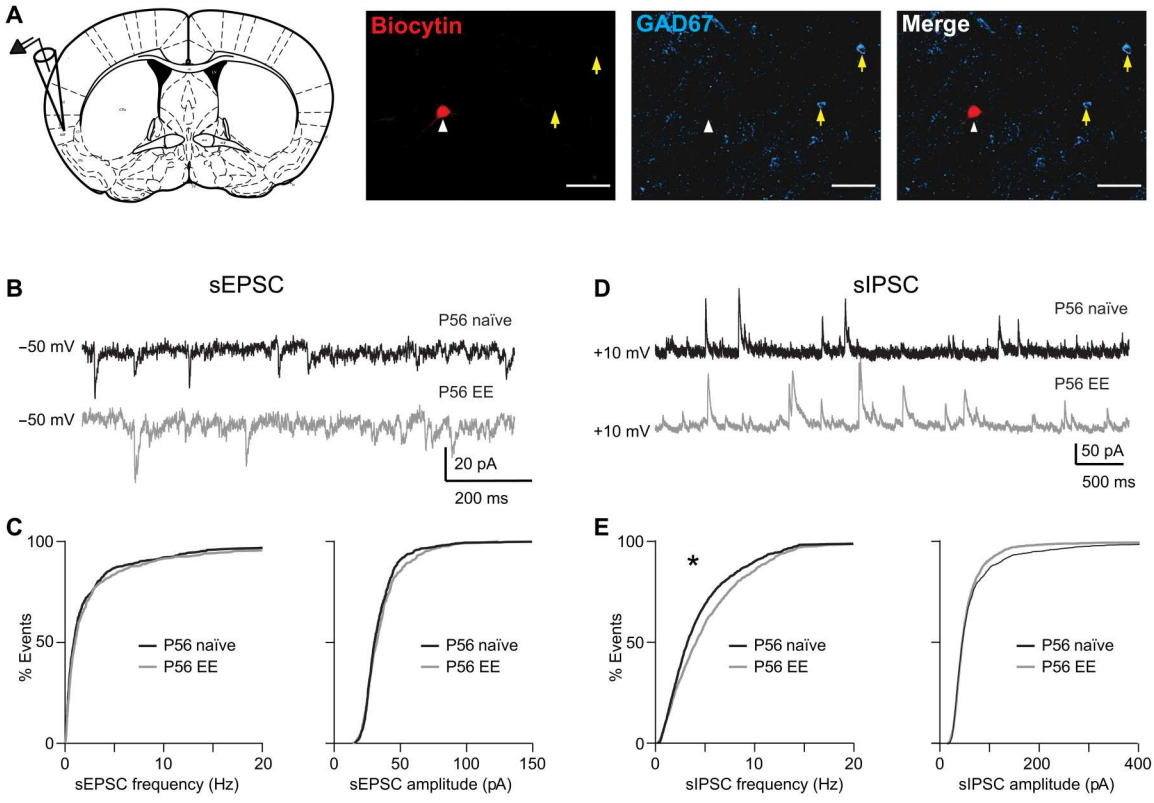

Fig. 4. Taste experience modulated inhibitory synaptic transmission in GC. (**A**) Left: Diagram of recording configuration and location of GC. Right: Example of recorded neuron lacking GAD67 immunostaining. Red, biocytin-filled neuron soma imaged through a single *z* plane; cyan, GAD67 immunostaining. White arrowhead, recorded neuron; yellow arrows, GAD67-expressing neurons. Scale bars, 50 μm. (**B**) Sample traces of sEPSCs in mice from naïve (black) and EE (gray) groups. Neurons were held at −50 mV, the reversal potential for Cl^-, during recordings. (**C**) Left: Cumulative distribution of sEPSC instantaneous frequency (P = 0.232, K-S test). Right: Cumulative distribution of sEPSC amplitude (P = 0.455, K-S test). (**D**) Sample traces of sIPSCs in mice from naïve (black) and EE (gray) groups. Neurons were held at +10 mV, the reversal potential for cations, during recordings. (**E**) Left: Cumulative distribution of sIPSC instantaneous frequency ($P = 9.24 \times 10^{-12}$, K-S test). Right: Cumulative distribution of sIPSC amplitude (P = 0.137, K-S test). Asterisk indicates $P \leq 0.01$.

respectively) were obtained by holding neurons at the reversal potential for chloride (−50 mV in our experimental conditions) or for α-amino-3hydroxy-5-methyl-4-isoxazolepropionic acid (AMPA)- and *N*-methyl-D-aspartate (NMDA) receptor–mediated currents (+10 mV; Fig. 4, B and D). Following EE, at P56, there were no significant changes in sEPSC frequency and amplitude (Fig. 4, B and C; naïve, n = 15 cells from 10 mice; EE, n = 14 cells from 11 mice; frequency: D = 0.0539, P = 0.232; amplitude: D = 0.0651, P = 0.455, K-S test), while we observed a significant increase in sIPSC frequency but not amplitude (Fig. 4, D and E; P56: naïve, n = 16 cells from 8 mice; EE, n = 15 cells from 12 mice; sIPSC frequency: D = 0.130, P = 9.24 × 10−12, K-S test; sIPSC amplitude: D = 0.0416, P = 0.137, K-S test). The effect of EE on inhibitory transmission was already detectable at P35 (fig. S8, A and B) and persisted at least until P56 (Fig. 4, D and E). The increase in sIPSC frequency at P35 was accompanied by an increase in sEPSC frequency (fig. S8C) and a decrease in sEPSC amplitude (fig. S8D), suggesting that, in the first few days following EE, both excitatory and inhibitory plasticity were engaged, but that over long temporal windows, only inhibitory plasticity persisted. These results suggest that increased inhibitory synaptic transmission underlies the decreased activation of putative PYR neurons, possibly contributing to modulating sucrose responsiveness and preference.

Taste experience modulated anatomical markers of inhibitory maturation in GC

To further investigate the effect of EE on inhibitory circuits in GC, we quantified anatomical markers, focusing on PV immunofluorescence and the accumulation of perineuronal nets (PNNs), extracellular matrix proteins that preferentially accumulate around PV^+ neurons (*33*–*35*). Changes in PV immunofluorescence have been associated with the effects of postnatal experience (*36*) and learning-related plasticity in adult animals (*37*), whereas the accumulation of mature PNNs is associated with the duration of sensitive periods for experience-dependent plasticity (*34*) and limits the capacity for inhibitory plasticity (*35*). To determine whether EE affected PV immunofluorescence and/or PNN accumulation, we used immunohistochemistry with an antibody against PV and incubation with *Wisteria floribunda* agglutinin (WFA) to label PNNs in wild-type C57BL/6 mice (Fig. 5, A and B). We quantified the intensity of PV and WFA fluorescence from individual PV^+ neurons and PNNs, as well as the proportion of PV^+ neurons associated with a PNN in naïve and EE mice. In GC of naïve mice, the proportion of PV^+ relative to all neurons was stable from P35 to P56 [Fig. 5C; P35, n = 5 mice; P56, n = 4 mice; $t_{(7)}$ = 0.7685, P = 0.467; unpaired two-tailed t test], as was the PV fluorescence intensity of neurons with and without a PNN (fig. S9, A and B). There was also no difference

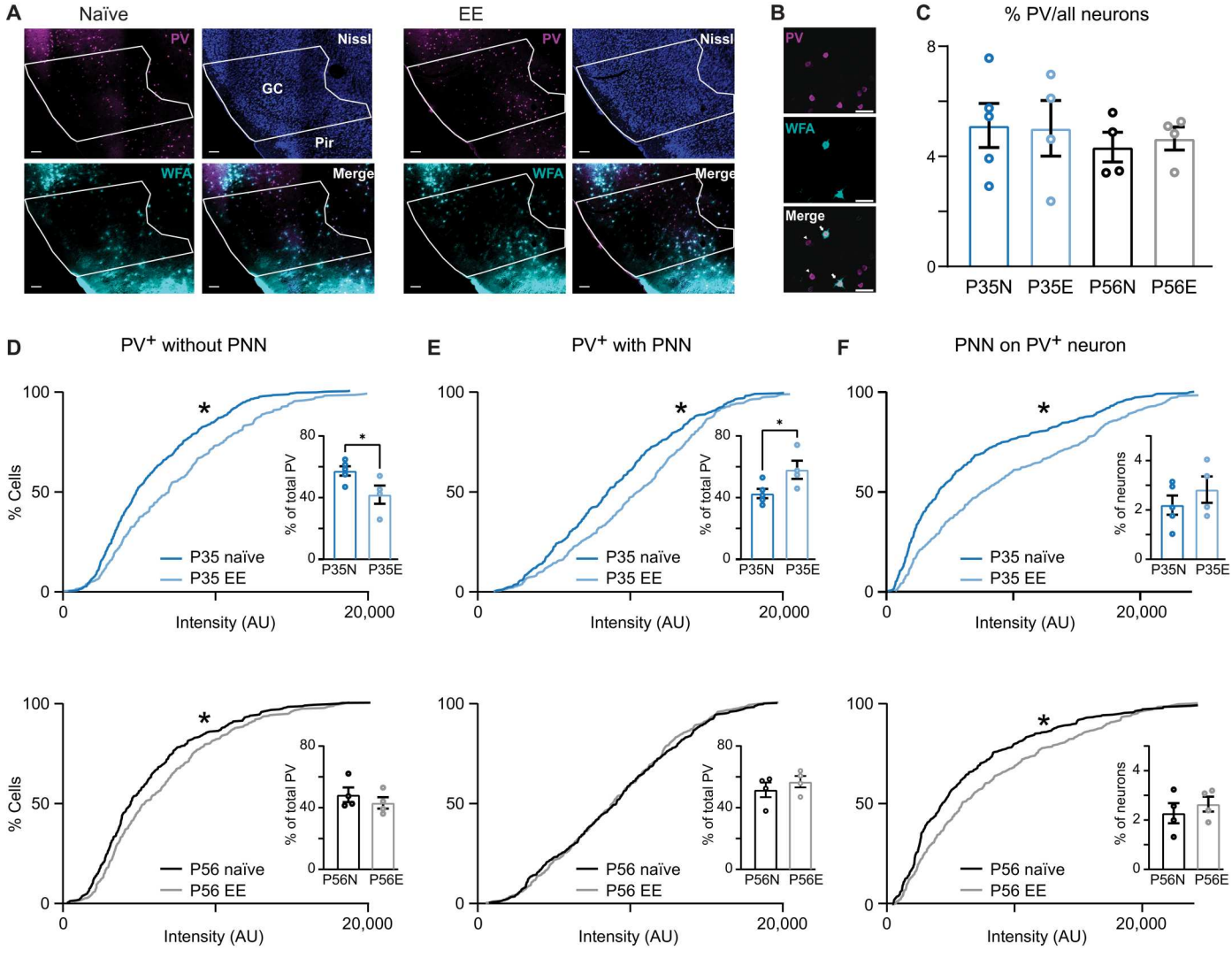

Fig. 5. PV$^+$ neurons and PNNs are modulated by EE. (**A**) Example images of GC sections stained with *Wisteria floribunda* agglutinin (WFA) (cyan) in naïve (left) and EE (right) mice. Scale bars, 100 μm. White masks, GC. Top right: PV immunostaining (magenta); bottom right: WFA staining for PNNs (cyan); top left: Nissl (blue); bottom left: merged images. (**B**) Zoomed-in view of a naïve section. Arrows, double-labeled neurons (PV + PNN); arrowheads, examples of PV$^+$ neurons without a PNN. Top: PV immunostaining (magenta); middle: WFA labeling of PNNs (cyan); bottom: merged images. Scale bars, 50 μm. (**C**) The proportion of PV$^+$ neurons in GC was stable across age groups and EE. Naïve, P35 versus P56 ($P = 0.467$, *t* test); EE, P35 naïve versus P35 EE, $P = 0.939$, *t* test; P56 naïve versus P56 EE, $P = 0.661$, *t* test. (**D**) Cumulative distribution of PV immunofluorescence intensity for PV$^+$ neurons without a PNN and bar plot of the proportion of PV$^+$ neurons lacking a PNN. Top: PV immunofluorescence signal at P35 ($P = 7.99 \times 10^{-6}$, K-S test); inset: proportion of PV$^+$ neurons lacking a PNN. Bottom: PV immunofluorescence signal at P56 ($P = 0.016$, K-S test); inset: proportion of PV$^+$ neurons lacking a PNN. (**E**) Cumulative distribution of PV immunofluorescence intensity for PV$^+$ neurons with a PNN and bar plot of proportion of PV$^+$ neurons with a PNN. Top: PV immunofluorescence at P35 ($P = 2.467 \times 10^{-5}$, K-S test); inset: proportion of PV$^+$ neurons with a PNN ($P = 0.042$, *t* test). Bottom: PV immunofluorescence of PV$^+$ neurons with a PNN at P56 ($P = 0.745$, K-S test); inset: proportion of PV$^+$ neurons with a PNN ($P = 0.416$, *t* test). (**F**) Cumulative distribution of WFA fluorescence intensity for PNNs associated with PV$^+$ neurons and proportion of PNNs associated with PV$^+$ neurons. Top: WFA fluorescence at P35 ($P = 2.555 \times 10^{-8}$, K-S test); inset: proportion of PNNs ($P = 0.363$, *t* test). Bottom: WFA fluorescence at P56 ($P = 8.869 \times 10^{-4}$, K-S test); inset: proportion of PNNs ($P = 0.497$, *t* test). Asterisks indicate $P \leq 0.05$.

in the proportion of PV$^+$ neurons associated with a PNN (fig. S9, A and B, insets), in WFA fluorescence intensity (fig. S9C), and in the proportion of PNNs (fig. S9C inset) in P35 and P56 naïve mice. These data indicate that PV immunofluorescence and accumulation of PNNs of naïve mice reached stable levels in the age range of P35 to P56.

EE did not affect the proportion of PV$^+$ neurons at P35 nor at P56 [Fig. 5C; P35 naïve, $n = 5$ mice; P35 EE, $n = 4$ mice; $t_{(7)} = 0.079$, $P = 0.939$; P56 naïve, $n = 4$ mice; P56 EE, $n = 4$ mice; $t_{(6)} = 0.4606$, $P = 0.661$, two-tailed unpaired *t* test]. However, there was a significant experience-dependent increase in the intensity of immunofluorescence signals for PV. Specifically, EE enhanced PV immunofluorescence in PV$^+$ neurons lacking a PNN both at P35 and P56 (Fig. 5D; P35 naïve, $n = 503$ neurons from five mice; P35 EE, $n = 289$ neurons from four mice; $D = 1.84$, $P = 7.99 \times 10^{-6}$; P56 naïve, $n = 316$ neurons from four mice; P56 EE, $n = 283$ neurons from

four mice; $D = 0.127$, $P = 0.016$, K-S test), pointing to long-lasting experience-dependent changes in PV expression in this group of PV^+ neurons. However, PV^+ neurons associated with a PNN showed enhanced PV immunofluorescence only at P35 (Fig. 5E; P35 naïve, $n = 382$ cells from 5 mice; P35 EE, $n = 378$ cells from four mice; $D = 0.173$, $P = 2.467 \times 10^{-5}$; P56 naïve, $n = 343$ cells from four mice; P56 EE, $n = 385$ cells from four mice; $D = 0.050$, $P = 0.745$, K-S test), suggesting that once PNNs accumulate, PV intensity stabilizes.

EE also affected the association of PV^+ neurons with PNNs. At P35, EE led to an increase in the proportion of PV^+ neurons with a PNN [Fig. 5, D and E, top, insets; P35 naïve, $n = 5$ mice; P35 EE, $n = 4$ mice; $t_{(7)} = 2.479$, $P = 0.042$, two-tailed unpaired t test]. This effect was not observed in EE mice tested at P56 [Fig. 5, D and E, bottom, insets; P56 naïve, $n = 4$ mice; P56 EE, $n = 4$ mice; $t_{(6)} = 0.8727$, $P = 0.416$, two-tailed unpaired t test], suggesting that EE accelerated the transition from lacking a PNN to having a PNN. These results suggest that the expression of PV in PV^+ neurons lacking a PNN continues to be modulated by experience at least until P56. Differently, the expression of PV in PV^+ neurons with a PNN reached stable levels by P56 and was not modulated by experience.

In addition to modulating PV immunofluorescence, EE enhanced PNN aggregation, detected as augmented fluorescence intensity of PNNs around PV^+ neurons. This effect was observed at both P35 and P56, compared to age-matched naïve mice (Fig. 5F; top: P35 naïve, $n = 5$ mice; P35 EE, $n = 4$ mice; $D = 0.219$, $P = 2.555 \times 10^{-8}$; P56 naïve, $n = 4$ mice; bottom: P56 EE, $n = 4$ mice; $D = 0.146$, $P = 8.869 \times 10^{-4}$, K-S test), even in the absence of changes in the proportion of PNNs in GC [Fig. 5F, insets; P35 naïve, $n = 5$ mice; P35 EE, $n = 4$ mice; $t_{(7)} = 0.9735$, $P = 0.363$; P56 naïve, $n = 4$ mice; P56 EE, $n = 4$ mice; $t_{(6)} = 0.7233$, $P = 0.497$, two-tailed unpaired t test]. These findings indicate that taste experience at the time of weaning regulates the state of maturation and the capacity for plasticity of PV^+ neurons. The effect of EE on PV immunofluorescence was long-lasting in PV^+ neurons lacking a PNN, while it was transient in PV^+ neurons with a PNN, suggesting that, once this group of inhibitory neurons accumulates a PNN, the expression of PV becomes insensitive to taste experience. In addition, the effect of EE on PNN aggregation, measured as WFA intensity, was persistent, indicating that taste experience regulates inhibitory plasticity in GC through distinct mechanisms.

PNN accumulation regulated the duration of plasticity for sucrose preference

Studies in flies and mice show that some forms of taste-dependent plasticity, such as conditioned taste aversion learning and some forms of taste discrimination, persist throughout life (*38*). Here, we asked whether the experience-dependent modulation of sweet preference that we report is specific to the early postnatal period or whether it persists throughout life. To investigate this, we tested whether our taste exposure paradigm would induce a shift in the sucrose preference curve if started in adult mice. For these experiments, mice were reared on a regular diet of chow and water until P56 and then exposed to the battery of taste solutions for 8 days starting at P57 [late exposure (LE); Fig. 6A]. Sucrose curves were obtained with BAT 4 weeks after the end of LE (at P91). Sucrose preference was unaffected by LE [Fig. 6A; naïve, $n = 10$ mice; LE, $n = 8$ mice; sucrose curve: $F_{(3,173)} = 1.130$, $P = 0.338$, F test; slope: $t_{(16)} = 1.144$, $P = 0.269$, two-tailed unpaired t test], indicating that the experience-dependent modulation of sucrose preference is developmentally restricted.

To determine whether the window for experience-dependent plasticity depends on GC inhibitory circuits and/or on accumulation of PNNs, we used a GC-restricted enzymatic removal of PNNs in adult mice and asked whether this manipulation could restore the experience-dependent shift in sucrose preference curve. The control group received bilateral intra-GC infusions of penicillinase (Pen), an enzyme that does not affect PNNs (*39*), while the experimental group received intra-GC bilateral infusions of chondroitinaseABC (chABC), an enzyme that breaks the bonds between PNNs proteoglicans, via chronically implanted cannulae. We first quantified the degree of degradation and the timing of PNN recovery following a chABC injection in GC. A single infusion of chABC in GC at P55 did not affect the proportion of PV^+ neurons quantified either 2 or 10 days after infusion, corresponding to the beginning and end of the exposure period [Fig. 6, B and C, left; 2 days: Pen, $n = 3$ mice; chABC, $n = 3$ mice; $t_{(4)} = 1.631$, $P = 0.178$; 10 days: Pen, $n = 3$ mice; chABC, $n = 3$ mice; $t_{(4)} = 0.625$, $P = 0.566$, two-tailed unpaired t test]. However, it was sufficient to degrade PNNs, which did not recover for over 10 days, in line with previous studies [Fig. 6, B and C, right; % PV^+ neurons associated with a PNN: 2 days: Pen, $n = 3$ mice; chABC, $n = 3$ mice; $t_{(4)} = 2.986$, $P = 0.041$; 10 days: Pen, $n = 3$ mice; chABC, $n = 3$ mice; $t_{(4)} = 5.794$, $P = 0.004$, two-tailed unpaired t test] (*40*). In the same mice, we confirmed that chABC degradation of PNNs was restricted to GC and did not affect piriform cortex, an important control given that olfaction contributed to the experience-dependent shift in sucrose preference (see Fig. 2C). In this region, neither the proportion of PV^+ neurons nor the proportion of PV^+ neurons with a PNN was affected (fig. S10). Following this validation, separate groups of mice received bilateral GC infusions of Pen or chABC at P55 and were then assigned to either naïve or LE group at P57 (Fig. 6, D to G). At the end of the exposure, LE mice returned to their regular diet of chow and water. Sucrose preference curves were obtained at P91 from four groups of mice: Pen-naïve, Pen-LE, chABC-naïve, and chABC-LE (Fig. 6, F and G). Pen-injected mice showed no change in their sucrose preference curves following LE [Fig. 6F; Pen-naïve, $n = 8$ mice; Pen-LE, $n = 8$ mice; sucrose curve: $F_{(3,137)} = 1.893$, $P = 0.134$, F test; slope: $t_{(14)} = 1.480$, $P = 0.161$, two-tailed unpaired t test]. However, LE was effective at shifting the sucrose preference curve in mice injected with chABC [Fig. 6G; chABC-naïve, $n = 7$ mice; chABC-LE, $n = 9$ mice; sucrose curve: $F_{(3,137)} = 42.89$, $P = 2.45 \times 10^{-9}$, F test; slope: $t_{(14)} = 8.515$, $P = 6.576 \times 10^{-7}$, two-tailed unpaired t test]. These results demonstrate that removal of PNNs locally in GC is sufficient to restore the experience-dependent modulation of sucrose curves in adult mice, indicating that GC is a locus of experience-dependent plasticity and that mature inhibition in GC constrains experience-dependent changes in sucrose preference.

Removal of PNNs in adult GC restored the capacity for plasticity of inhibitory synapses

We next asked whether removal of PNNs in GC also restored the experience-dependent increase of inhibitory synaptic transmission onto PYR neurons. For these experiments, mice received a bilateral intra-GC injection of chABC at P56 and were then assigned to either the naïve or LE group beginning at P57. At P91, 4 weeks after the end of LE, acute slices containing GC were obtained,

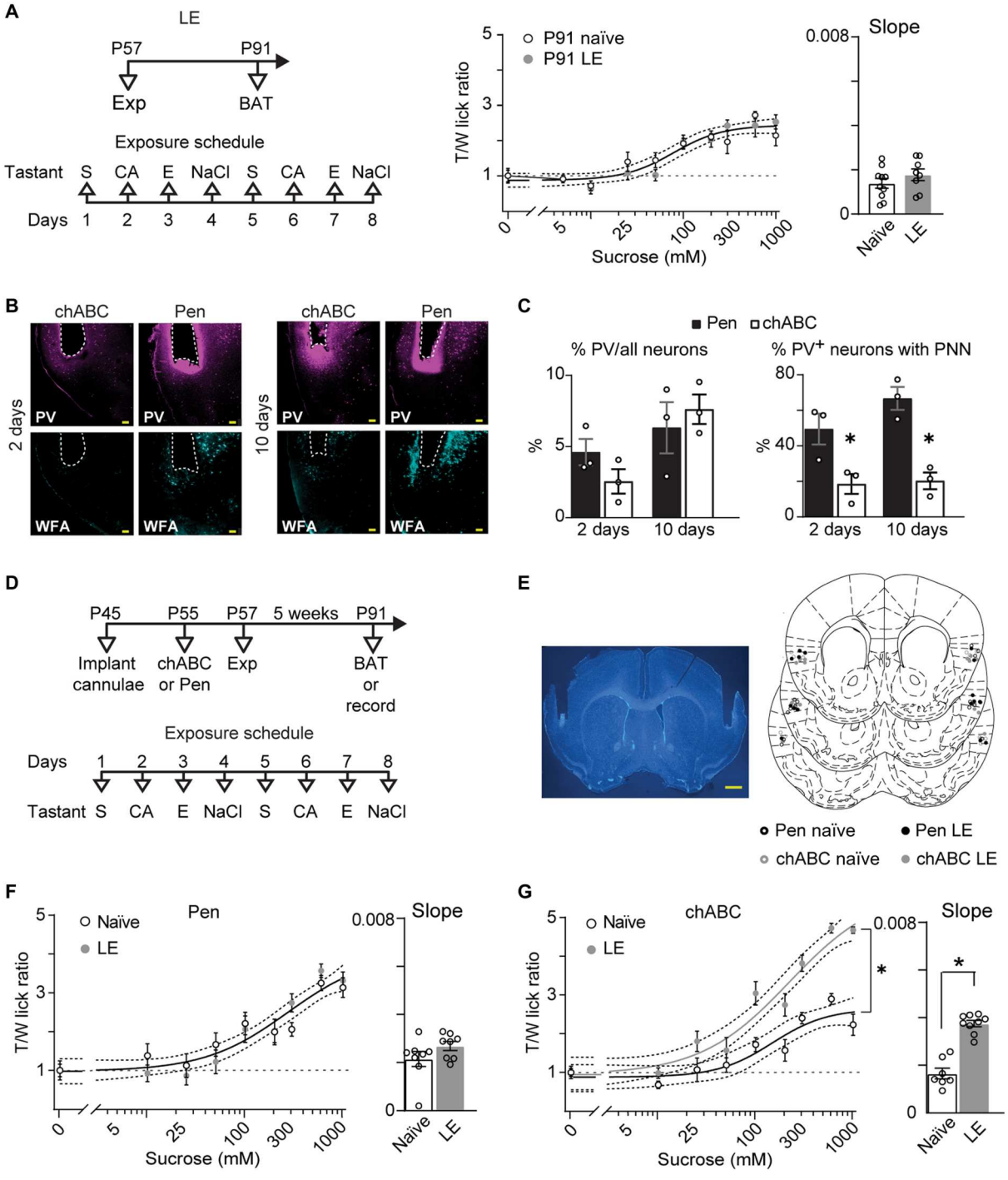

Fig. 6. PNN degradation in GC restored sensitivity to taste experience and plasticity of inhibition in adult mice. (**A**) Left: Schedule of LE (top) and sequence of tastants (bottom). Middle: Sucrose preference curves for naïve and LE mice tested at P91. A single curve fitted both datasets ($P = 0.338$, F test). Right: Slope of sucrose curve for naïve (white) and LE (gray) mice ($P = 0.269$, two-tailed unpaired t test). (**B**) Representative images of sections immunostained for PV (magenta) and WFA (cyan) following GC infusion of chABC or Pen. Scale bars, 100 μm. (**C**) Quantification of PV^+ neurons and PV^+ neurons with a PNN 2 and 10 days after infusion. Infusion of chABC did not affect the number of PV^+ neurons (2 days: $P = 0.178$, t test; 10 days: $P = 0.566$, t test); however, it reduced the number of PV^+ neurons with a PNN (2 days: $P = 0.041$, t test; 10 days: $P = 0.004$, t test). (**D**) Top: Experimental schedule for cannulae implant, LE, and BAT. Bottom: Sequence of taste solutions. (**E**) Left: Representative cannulae placement in GC; brain section stained with Hoechst 33342; scale bar, 500 μm. Right: Cannulae placements for all mice registered to sections of the mouse brain atlas (from bregma: +1.34, +1.10, and +0.74 mm). (**F**) Left: Sucrose preference curves from P91 mice infused with Pen in naïve (black open circles) or LE (gray filled circles) groups (single curve fit both datasets: $P = 0.134$, F test). Right: Slope of sucrose curve for Pen naïve (white) and Pen LE (gray) mice ($P = 0.161$, two-tailed unpaired t test). (**G**) Left: Sucrose curves for mice infused with chABC in naïve (black open circles) versus LE (gray filled circles) group (separate curves fit the datasets: $P = 2.45 \times 10^{-9}$, F test). Right: Slope of sucrose curve for chABC naïve (white) and chABC LE (gray) mice ($P = 6.576 \times 10^{-7}$, two-tailed unpaired t test). Asterisks indicate $P \leq 0.05$.

and patch clamp recordings were used to record sIPSCs (Fig. 7, A and B). We observed an increase in sIPSC frequency (Fig. 7B, left; chABC-naïve, $n = 20$ cells from 3 mice; chABC-LE, $n = 14$ cells from 5 mice; $D = 0.166$, $P = 3.199 \times 10^{-20}$, K-S test) and a small, but significant, increase in sIPSC amplitude (Fig. 7B, right; chABC-naïve, $n = 20$ cells from 3 mice; chABC-LE, $n = 14$ cells from 5 mice; $D = 0.089$, $P = 4.407 \times 10^{-6}$, K-S test) in neurons from chABC-LE mice, indicating that removal of PNNs in adult mice allowed for an LE-induced increase in inhibitory synaptic transmission comparable to what we observed following EE. To assess whether the combination of chABC and LE affected the E/I balance, we also measured sEPSC amplitude and frequency from the same neurons. In chABC-LE mice, we observed a significant increase in sEPSC frequency with no change in sEPSC amplitude compared to chABC-naïve mice (Fig. 7, C and D; chABC-naïve, $n = 19$ cells from 3 mice; chABC-LE, $n = 13$ cells from 5 mice; frequency: $D = 0.208$, $P = 1.452 \times 10^{-10}$; amplitude: $D = 0.089$, $P = 0.027$, K-S test). The increase in sEPSCs frequency is comparable to that observed at P35 following EE and suggests that complete enzymatic removal of PNNs may bring the GC circuit back to a juvenile developmental stage that is permissive for plasticity over several weeks.

These data, together with the observations in young mice showing a persistence of inhibitory plasticity long after the end of the exposure paradigm, support the interpretation that accumulation of PNNs around PV^+ neurons in GC limits the capacity for plasticity of inhibitory synapses and prevents the experience-dependent shift in sucrose preference from occurring in adulthood. Thus, the maturation of inhibitory circuits provides a limiting factor that restricts experience-dependent modulation of sweet preference to the first few weeks of postnatal development.

DISCUSSION

We have shown that taste experience at the time of weaning not only influences the preference for sweet in adults but also profoundly modulates the postnatal development of gustatory cortical circuits. A convergence of chemosensory signals, nutrient variety, and post-ingestive signals contributes to the experience-dependent shift in sweet preference, highlighting the central role for GC in the integration of sensory information related to feeding. The dilution of powdered Ensure that we used (1 g of Ensure powder to 10 ml of water) contained 228 mg of sugars, which is about one-half of the sugar content in the 150 mM sucrose solution (513.45 mg in 10 ml). The calorie content of the Ensure solution that we used was 4.1 kcal in 10 ml (0.9 kcal from sugars), while the calorie content of the 150 mM sucrose solution was 2.05 kcal in 10 ml (all of them from sugars). The order of magnitude of the sugar amount and calorie content is comparable in the two solutions. Therefore, it is unlikely that calories from sugar alone would be sufficient to drive the shift in sweet preference. Ensure also contains carbohydrates

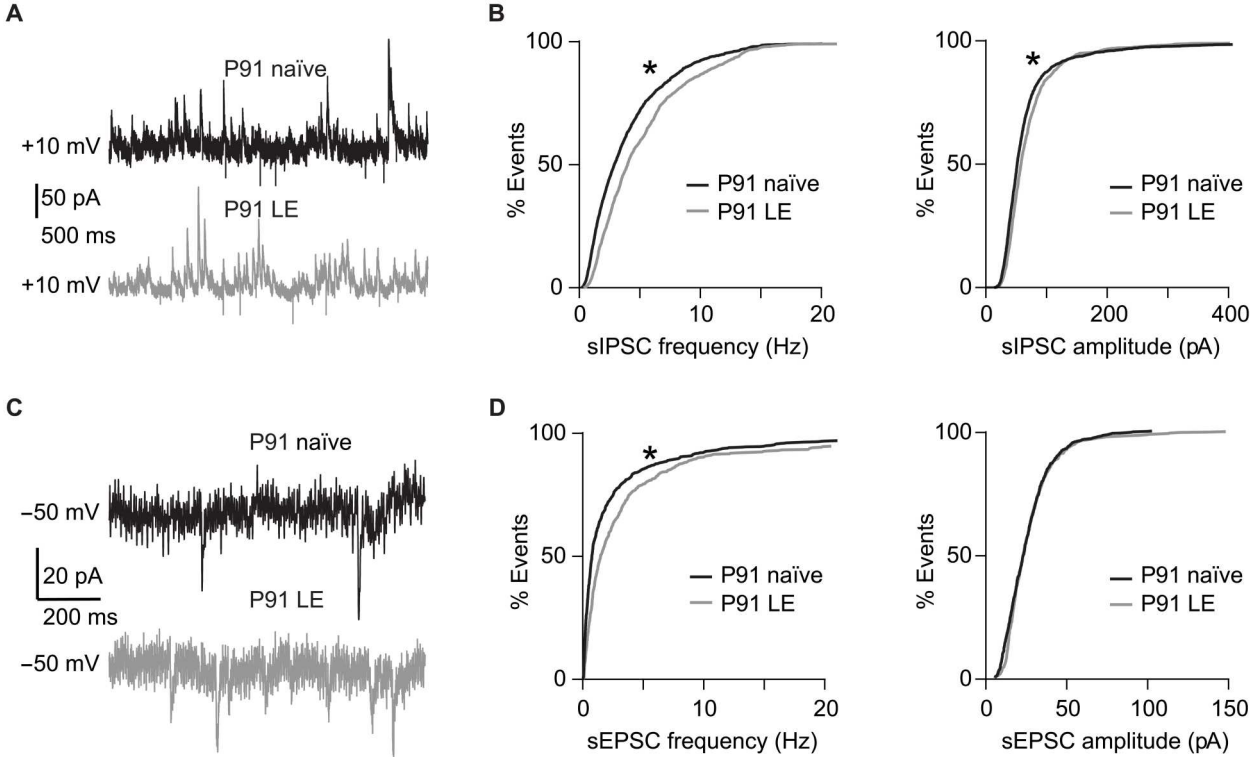

Fig. 7. Removal of PNNs restores the capacity for inhibitory plasticity following LE. (**A**) Sample traces of sIPSCs recorded from slices obtained from mice infused with chABC in GC at P55 recorded at P91. chABC injected mice were grouped in naïve (black) and LE (gray) cohorts. (**B**) Left: Cumulative distribution of sIPSCs frequency for chABC-naïve (black) and chABC-LE (gray) mice ($P = 3.199 \times 10^{-20}$, K-S test). Right: Cumulative distribution of sIPSC amplitude for chABC naïve and chABC-LE groups ($P = 4.407 \times 10^{-6}$, K-S test). (**C**) Sample traces of sEPSCs recorded from slices obtained from mice infused with chABC in GC at P55 recorded at P91. chABC injected mice were grouped in naïve (black) and LE (gray) cohorts. (**D**) Left: Cumulative distribution of sEPSCs frequency for chABC-naïve (black) and chABC-LE (gray) mice ($P = 1.452 \times 10^{-10}$, K-S test). Right: Cumulative distribution of sEPSC amplitude for chABC naïve and chABC-LE groups ($P = 0.027$, K-S test). Asterisks indicate $P \leq 0.01$.

(fructo-oligosaccharides), proteins, and fats, which engage postingestive processes differently than sugar alone, as well as minerals and vitamins. Thus, in view of the finding that 8 days of sugar did not shift the preference curve, but 8 days of Ensure did, the most parsimonious explanation for the effect that we report is that it depends on the convergence of experience with chemosensation (taste and olfaction) of a variety of tastes and nutrients, as well as their calorie content.

An intact olfactory epithelium during EE is necessary for the shift in sweet preference. Temporary anosmia during EE impairs the plasticity of preference even if the sense of smell has fully recovered before testing day. These results point to the need for interactions between taste and olfaction during exposure. In support of this interpretation, there is evidence of responses to intraoral odor solutions, tastes, or somatosensory stimuli both in olfactory cortex and GC (*41*, *42*), as well as of the influence of GC on the olfactory cortex (*43*). The formation of a flavor percept involves retronasal smell during chemosensory experience, another factor that may contribute to shaping preference during development. Recent evidence points to the fact that retronasal odor perception requires GC activity in adult rodents (*44*), highlighting a central role for GC in the perception of flavor. Whether these findings extend to developing animals and are influenced by brief experience with tastants early in life will need further study.

Analysis of licking microstructure supports the interpretation that early taste experience increases the palatability and avidity for sucrose, as EE mice increase the duration of lick bouts and accumulate licks to sucrose faster than their naïve littermates. The increase in palatability bolsters the increase in preference and lends an explanation to why EE mice direct their licking to sucrose in the BAT. Whether this change in palatability renders sucrose more, or less, rewarding following EE remains to be determined.

We demonstrate in vivo that the change in sucrose preference is accompanied by increased spontaneous activity of PV^+ neurons, reduced spontaneous and sucrose-evoked activity in PYR neurons, and changes in responsiveness to sucrose concentrations of PYR neurons. Furthermore, our ex vivo data indicate that increased inhibitory synaptic drive onto GC PYR neurons is the likely mechanism regulating their responsiveness to sucrose. While we observed experience-dependent changes in both excitatory and inhibitory drive at P35, imaging experiments were performed at P56, when excitatory drive had stabilized, and only changes in synaptic inhibition were observed. Thus, the long-term effect of EE likely depends on inhibitory synaptic plasticity.

The experience-dependent changes that we report are specific for early experience with tastants and nutrients. The exposure paradigm applied to adult mice failed to shift the sucrose preference curve, indicating the presence of a sensitive window during which the gustatory experience can modulate the preference for sweet and neural activity. While critical period plasticity has been reported in a different and nonoverlapping portion of the insular cortex representing integration of auditory and visual inputs (*45*), the prevailing view to date has been that there is no sensitive window for taste (*46*). This assumption was based on reports of experience-dependent plasticity throughout life in rodent GC (*1*, *47*) and in flies taste neurons (*48*). Our data showing that taste behaviors can be modulated within restricted developmental windows provide possible behavioral and neural mechanisms underlying long-term effects of early-life taste experiences in humans (*2*, *3*) and center GC as a locus of experience-dependent plasticity.

In this study, we focused on GC for its role in taste processing and taste-related behaviors. However, taste experience influences the development of other circuits along the taste axis, including the nucleus of the solitary tract (NTS) (*49*). The inputs via cranial nerves terminating in the NTS undergo maturation until P35, and the process remains incomplete in a salt-deficient diet, indicating the requirement for early taste experience in the development of the taste system (*50*). These published results raise the possibility that the effects that we observed rely on indirect GC modulation by other brain regions along the taste system. Previous work reported that removal of GC does not affect the palatability of tastants and only mildly impairs simple taste discriminations (*51*–*53*). These findings were interpreted as evidence that GC is not required for taste identification or palatability. Contrary to these assumptions, our data demonstrate that GC, particularly its inhibitory circuits, plays a crucial role in the experience-dependent modulation of sweet preference. Local manipulation of PNNs in GC of adult mice was sufficient to restore the experience-dependent shift in sucrose preference curve and the increase in synaptic inhibition that we observed in younger mice. These results identify accumulation of PNNs around PV^+ neurons as a mechanism restricting experience-dependent inhibitory plasticity, generalizing findings from other sensory cortical areas to GC (*54*).

The expression of PV is activity dependent and sensitive to experience and learning in sensory cortex (*55*) and in the hippocampus (*56*). Furthermore, in the hippocampus, PV expression was correlated with changes in GABAA receptor expression (*57*) and with accumulation of PNNs (*58*). Last, PV regulates firing properties of GABA neurons in the thalamic reticular nucleus (*59*). Our work adds to this literature and extends it by showing that PV expression and PNN accumulation are sensitive to early dietary exposure and that the accumulation of PNNs in GC is sufficient to close a sensitive window for the plasticity of taste preference. As PV is a calcium-binding protein, changes in its expression levels are likely to affect GABA release and, possibly, plasticity mechanisms. Our data, when interpreted in the context of previous findings from several brain regions, strongly suggest that the effect of EE on PV expression, PNN accumulation, and GABA transmission results in the shift in E/I activation we report in GC.

While we cannot exclude the contribution of other inhibitory neuron types to the increase in sIPSCs frequency, our data provide evidence that PV^+ neurons are the likely contributors to the increase in sIPSCs. The largest proportion of spontaneous synaptic events recorded in patch clamp configuration typically originates from the perisomatic area of the neuron, where most inhibitory synapses come from PV^+ neurons (*60*). Published literature (*61*), including several publications from our group (*62*, *63*), demonstrated the involvement of PV^+ neurons in experience-dependent plasticity. There is also substantial published evidence, confirmed by our own quantification, that PNNs almost exclusively associate with PV^+ neurons (*34*), and PNNs modulate the capacity for plasticity of PV^+ neurons (*39*). Furthermore, our data show that removing PNNs in adult mice restored the capacity for the increase in sIPSC frequency in adult mice. These factors, together with the changes in spontaneous activity that we observed in PV^+ neurons in vivo, support the interpretation that this group of inhibitory neurons contributes substantially to the effect of EE. Spontaneous

inhibitory currents can, of course, include events from synapses by other inhibitory neuron groups. However, most PV^- inhibitory neurons make connections with the dendritic regions of PYR neurons, and the amplitude of their responses recorded in patch clamp tends to be smaller, with slower kinetics due to dendritic filtering (*60*). Last, our results do not exclude that other circuits in the taste system, including inputs to GC, may be modulated by taste experience but highlight GC as an essential circuit driving the establishment of sweet preference during postnatal development.

Absence of taste experiences early in life, as is the case for tube-fed preterm infants, may have long-term deleterious effects on brain development (*64*). In addition, children with neurodevelopmental disorders are often picky eaters (*65*); show hypersensitivity to certain aspects of the taste experience, including smell, texture, and aftertaste (*66*); and tend to show food selectivity (*67*). Furthermore, many neurodevelopmental disorders show comorbidity with gastrointestinal symptoms associated with the composition of the gut microbiome, which, in turn, can modulate neurotransmitter levels (*68*), including GABA (*69*). Our findings highlight the importance of early experience with food and tastants not only for the development of food preferences in adulthood but also for the postnatal maturation of cortical circuits and sensory processing, providing evidence of the influence of chemosensation and early dietary exposure for brain function.

MATERIALS AND METHODS

Animals

All experimental procedures followed the guidelines of the National Institute of Health and were approved by the Institutional Animal Care and Use Committee at Stony Brook University. Mice of both sexes were housed in a vivarium on a 12-hour light-dark cycle. All mice were group-housed except for a subset of mice tested in control assessments of baseline tastant consumption (fig. S1, A and B; naïve, $n = 4$; EE, $n = 3$) and for mice used for two-photon imaging experiments (Fig. 3 and figs. S5 and S6; naïve, $n = 5$; EE, $n = 5$), which were single-housed following surgery for the prism implant. Experiments were performed during the light cycle. Wild-type C57Bl/6 mice were purchased from Charles River Laboratories to arrive either as adults or as litters, including the lactating mother and pups at P5. *PV-cre* (*23*) (JAX stock no. 017320) and *Ai14* (*24*) (RRID: IMSR_JAX:007908) were ordered from the Jackson Laboratory and crossed in our animal facility. The *PV-cre;Ai14* mice were heterozygous for both *Cre* and *Lox-Stop-Lox-tdTomato* alleles and were bred in-house by crossing female homozygous PV-cre mice with males homozygous for the *Ai14* reporter gene.

Behavioral procedures

Exposure

Exposure began at P22 for the EE group and P57 for the LE group. The animal's home cage water bottle was replaced with a taste solution following an 8-day schedule [Fig. 1A; 150 mM sucrose (S) on days 1 and 5, 20 mM citric acid (CA) on days 2 and 6, Ensure (E) on days 3 and 7, and 100 mM salt (NaCl) on days 4 and 8]. Ensure was delivered in a bowl to eliminate the possibility of clogging the spout. Mice had ad lib access to chow. Control mice (naïve) remained on a diet of ad lib chow and water. For the calorie-free EE, the home cage water bottle was replaced with a taste solution with the following 8-day schedule: 8 mM saccharin on days 1 and 5, 20 mM citric acid on days 2 and 6, 100 mM MSG on days 3 and 7, and 100 mM salt on days 4 and 8. For experiments in which animals were given 8 days of either sucrose, salt, or Ensure, they were treated as above but with the appropriate taste solution.

Tube feeding

Tube feeding began on P22 and ended on P29. Polyurethane tubing (0.63 mm by 1.02 mm) was marked with the length from the mouth to the animal's sternum and attached to a 10-ml Hamilton syringe. Infusates were either water or Ensure. The concentration of Ensure was determined by calculating the amount of Ensure consumed during 1 to 2 hours access in the anosmia experiment (see below) to approximate the calorie intake by mice of a certain body weight. Ensure was then mixed to be more concentrated to accommodate the smaller volume delivered by tube feeding. The concentrated Ensure was administered up to three times per day. The exact concentration was calculated for each animal's body weight on each day. The highest concentration was 6 g/ml. Animals were scruffed and the tubing gently inserted into the mouth and down the esophagus until the necessary length of tubing was inserted. Infusate was then slowly administered by hand using a syringe at approximately 0.1 ml/10 g bodyweight. Animals were monitored after infusions for signs of aspiration or discomfort, neither of which were observed.

Intranasal instillation for anosmia

Intranasal instillations of $ZnSO_4$ or saline were performed as previously described with modifications for weanlings (*70*). To determine the appropriate length for the infusion apparatus and volume of infusate, a pilot experiment was conducted in which Alexa Fluor 488 dye transport was observed from the nasal epithelium to the olfactory bulbs without expulsion or aspiration of infusate. For experimental animals, P21 mice were lightly anesthetized with a cocktail of ketamine (70 mg/kg) and dexmedetomidine (1 mg/kg). Eppendorf microloaders were attached to a 1-μl Hamilton syringe. Animals were placed on their side while a microloader was threaded 5 mm into the naris. Animals were then rotated onto their back while 4 μl of infusate [$ZnSO_4$ (155 mM) or saline] was slowly administered. The mice remained in this position for 20 min, and then, they were rotated to their opposite side. After a 5-min delay, the same procedure was conducted for infusion into the opposite naris. Animals were then given antisedan (1 mg/kg) to reverse the dexmedetomidine. For delivery of Ensure for 8 days in $ZnSO_4$- or saline-treated mice, individual mice were transferred from their home cage to a holding cage containing standard bedding for 1 to 2 hours/day with access to a small bowl of Ensure. The amount of Ensure consumed on each day was measured by weighing the bowl before and after consumption. This procedure allowed us to measure the amount of Ensure consumed by individual mice while maintaining group housing.

Brief access test

Procedures were adapted from Glendinning *et al.* (*71*). Sucrose preference curves were collected using a commercially available gustometer (Med Associates Inc., Davis Rig for Mouse-16 Bottle). The apparatus consisted of a chamber (14.5 cm wide, 30 cm deep, and 15 cm tall), a motorized moving table to deliver multiple taste stimuli, a motorized shutter door to allow temporary delivery of tastants, and a dedicated computer to control tastant delivery and to record the timing of licks. Licks were detected by a high-frequency ac contact circuit activated by tongue contact with the sipper tube. The apparatus was cleaned with 70% ethanol between mice.

The number of licks, the latency to the first lick, and inter-lick intervals (ILIs) were recorded for each trial. For analysis, ILIs of <60 ms were removed to exclude double contacts occurring from a single tongue protrusion (*71*). Water restriction began on day 1 of training. Water restriction parameters were mild to minimize thirst-driven consumption and to maximize licking due to the appetitive nature of sucrose. Mice were weighed daily to ensure maintenance of at least 80% of their initial body weight. Table 1 summarizes the schedule of training and access to water.

On day 1 of training, mice were habituated to the Davis rig gustometer in a 30-min session where the shutter door remained open and granted access to a sipper tube connected to a bottle containing water. At the end of the first session, the water bottle was removed from the home cage and water restriction began.

On day 2, mice were returned to the gustometer for a 30-min spout training session. Once the mouse was placed in the chamber, the shutter opened, granting access to a sipper tube connected to a bottle containing water. Mice were allowed to lick ad libitum during the 30-min session. On day 3, mice were familiarized with the trial structure and the opening and closing of the shutter door (shutter training). These 30-min sessions consisted of trials in which the shutter door opened, granting access to a sipper tube connected to a bottle containing water. If the mouse did not lick, then the shutter door closed after 15 s, followed by a 5-s intertrial interval (ITI). If the mouse did lick, then the shutter door remained open for 10 s following the first lick. At the end of the 10-s interval, the shutter door closed. During the 5-s ITI, the motorized table moved to present a different bottle containing water. At the end of day 3, mice had 10-min access to a water bottle in their home cage. On days 4 and 5, mice were weighed and then given 5-min access to a water bottle in the home cage 2 hours before being placed in the gustometer for the acquisition of sucrose preference curves. At the end of day 4, mice had 10-min access to a water bottle in the home cage, while at the end of day 5, the experiment was concluded, and mice were returned to ad libitum access to water. On test days (4 and 5), the trial length was 10 s with a 5-s ITI. The shutter door closed after 10 s if the mouse did not lick. In this case, mice were presented the same bottle on the subsequent trial.

To obtain sucrose preference curves, six bottles containing different concentrations of sucrose were presented in a pseudorandom order. The range of concentrations was presented as a block, and the software randomized the presentation (without replacement) within each block. The sucrose concentrations presented on sucrose curve 1 were 0, 5, 10, 50, 100, and 600 mM, and those presented on sucrose curve 2 were 0, 5, 25, 200, 300, and 1000 mM. Sucrose curve 1 or 2 was presented on either day 4 or 5 of testing, ensuring that presentation was counterbalanced within groups. Mice in the EE group were P56 on day 4; mice in the LE group were P91 on day 4. For BAT for assessing salt preference, the salt concentrations presented on salt curve 1 were 0, 10, 50, 100, 250, and 500 mM, and those presented on salt curve 2 were 0, 25, 75, 400, 750, and 1000 mM. Salt curve 1 or 2 was presented on either day 4 or 5 of testing, ensuring that presentation was counterbalanced within groups. To assess saccharin preferences with BAT, the saccharin concentrations presented on saccharin curve 1 were 0, 0.2, 2, 10, and 20 mM, and those presented on saccharin curve 2 were 0, 0.6, 6, and 20 mM. Saccharin curve 1 or 2 was presented on either day 4 or 5 of testing, ensuring that presentation was counterbalanced within groups. For BAT following Pen or chABC infusion presented in Fig. 6 (F and G), 5 mM sucrose was omitted from testing. Mice had to participate in at least 20 trials to be included in the final analyses. For the sucrose preference curves collected at P56, 4 of a total of 93 mice used were removed from analysis because their average lick rate to water was less than 1 Hz.

Behavioral protocol for two-photon imaging

All procedures were conducted on a custom-designed behavioral apparatus controlled with codes written in LabView (National Instruments). Events were recorded on an Intan RHD USB Interface Board (RHD2000, Intan Technologies). Licks were detected using an electronic circuit (*72*). Following recovery from prism implantation surgery (see below), mice were placed on water restriction for 1 week (85% body weight, 1 to 1.5 ml of water daily). Next, they were habituated to perform five dry licks to receive one drop of water (4 μl) from a motorized spout (X-LSM, Zaber Technologies). The ITI for each session was 10 ± 4 s. If an animal failed to perform five dry licks within 3 s, then the spout retracted and an additional time-out of 10 s was triggered. After 4 days of habituation, two-photon imaging with sucrose concentrations began. Mice needed to perform five dry licks to receive one drop (4 μl) of either sucrose or water. The following concentrations of sucrose were used: 0 (water), 25, 50, 100, 200, and 600 mM. On each trial, a water rinse (4 μl) was given 8.3 ± 0.25 s after each taste. Tastants were delivered using gravity-fed solenoid valves (Lee Company) controlled by a ValveLink8.2 controller (AutoMate Scientific). Equal numbers of trials for each taste solution were delivered in a pseudorandom order. Mice were allowed to continue performing the task until they stopped licking (total trials: naïve, 109.9 ± 5.1; EE, 96.1 ± 6.1; t test, $P > 0.05$, $t = 1.673$, df = 25). The average lick rate across all tastants/conditions was comparable (fig. S6A; naïve: 0 mM, 8.5 ± 0.14; 25 mM, 8.5 ± 0.14; 50 mM, 8.5 ± 0.15; 100 mM, 8.5 ± 0.14; 200 mM, 8.6 ± 0.13; and 600 mM, 8.5 ± 0.15; EE: 0 mM, 8.7 ± 0.10; 25 mM, 8.7 ± 0.11; 50 mM, 8.7 ± 0.11; 100 mM, 8.6 ± 0.10; 200 mM, 8.7 ± 0.11; and 600 mM, 8.6 ± 0.10; two-way ANOVA sucrose concentration: $F = 3.03$, df = 1, $P > 0.05$; naïve versus EE: $F = 0.11$, df = 5, $P > 0.05$; interaction, $F = 0.04$, df = 5, $P > 0.05$), indicating similar levels of licking across conditions.

Buried food test

Mice were treated with intranasal instillations at P21. Behavior-tested procedures were modified from (*73*) and were video-recorded. Pre-exposure to Froot Loops began on P22 in their home cage for 3 days (P22 to P24) before testing. Testing took place on P25 or P28. The day before testing, chow was removed from the home cage at approximately 5 p.m. for an overnight food restriction. On test day, mice were individually transferred to a clean shoebox cage containing at least 3 cm of bedding and allowed to explore for 5 min. They were then removed from the test cage and returned to their home cage while one-quarter to one-third piece of Froot Loop was buried in the test cage. They were then returned to the test cage and placed in the half of the cage opposite to where the target Froot Loop was buried. The time to sniff in the correct location, dig in the correct location, and retrieve the pellet were recorded. Animals were allowed to explore and attempt to find the pellet for 15 min (900 s), at which point, time-out occurred, the pellet was unburied, and they were allowed to consume it. All mice quickly found and ate the pellet once unburied. Analysis was done on the time to dig in the location of the pellet.

Habituation/dishabituation

Anosmia and recovery from anosmia were assessed with a nonassociative behavioral task designed to assess the mouse's investigation of a novel odor [modified from (*74*)]. Mice were individually transferred from their home cage to a clean empty cage of the same size. On habituation trials, a hexagonal weigh boat containing a small piece of filter paper dipped in mineral oil was presented on the wire cage top such that the mouse could sniff and explore but not touch. Three 60-s habituation trials with mineral oil were presented with a 2-min ITI. In the final trial (also 60 s), mice were presented with a hexagonal weigh boat containing a small piece of filter paper dipped in methyl valerate (1:500 concentration diluted in mineral oil) or isoamyl acetate (1:500 concentration diluted in mineral oil). Time spent sniffing was included if the mouse was standing in the third of the cage containing the weigh boat and engaged in active sniffing directed toward the weigh boat.

Surgery

Implants of infusion cannulae

Mice aged P45 to P48 were anesthetized with an intraperitoneal injection of a cocktail containing ketamine (100 mg/kg) and xylazine (10 mg/kg). Bupivacaine (2.5 mg/ml, ~0.1 ml) was administered under the scalp for local anesthesia. Craniotomies were made over the left and right GC at the following coordinates: +1.0 mm anterior from bregma and 3.25 mm lateral from midline. Stainless steel guide cannulae (26 gauge, 5.0 mm, Plastics One) were lowered 1.8 mm vertical from the cortical surface and fixed to the skull with acrylic dental cement (Stoelting). A metal head post was implanted posterior to the cannulae for head restraint during infusion. Once the dental cement was completely dry, dummy cannulae were inserted into each guide cannula, and animals were allowed to recover for at least 1 week before the infusion. For the experiments examining the time course of recovery from the chABC (Fig. 6, B and C), surgical procedures were unilateral with a single cannula implant in the left GC. For experiments shown in Fig. 6, D to G, cannula implants were bilateral.

Injection of viral construct and prism implant

In preparation for two-photon imaging, *PV-cre;Ai14* mice underwent two surgeries. The first was performed at P20 or P21. Mice were anesthetized with the ketamine/xylazine cocktail described above, and a craniotomy was made over the left GC at the following coordinates: +0.8 mm from bregma and ~3.5 mm lateral from midline (close to the lateral suture). A pulled glass pipette attached to a 10-μl Hamilton syringe was backfilled with a solution containing a viral construct carrying gCaMP7f (*AAV1-syn-jGCaMP7f-WPRE*, titer 3×10^{13} genome copies (gc)/ml; Addgene, catalog no. 104488-AAV1). To reach the appropriate titer, the stock virus solution was diluted 1:4 in sterile saline. Injections were delivered at 1.75 and 1.9 mm below the pial surface. The syringe tip was slowly lowered in the brain to the desired depth, and a total volume of 225 nl was infused at a rate of 1 nl/s using a microinjection syringe pump (UMP3T-1, World Precision Instruments). The pipette tip was left in place for 10 min after each infusion before being slowly retracted. The craniotomy was filled with silicone (Dow Corning 200), and the skin suture-closed. Mice were given an injection of lactated Ringer's solution, placed back into the home cage, and allowed to recover overnight on a heating pad. The exposure paradigm began 1 to 2 days later at P22. A second surgery to implant prisms was performed at P42 to P44. Mice were anesthetized as described above and administered subcutaneous injections of dexamethasone (2 mg/kg) and carprofen (5 mg/kg) before beginning the surgery. Bupivacaine (2.5 mg/ml, ~0.1 ml) was administered under the scalp for local anesthesia. The skin above the skull and overlying the left temporalis muscle was removed and the skull cleaned. Portions of the temporalis muscle were removed, and an ~2.2 mm–by–2.2 mm craniotomy was opened on the lateral surface of the skull with a dental drill using the middle cerebral artery as a landmark for GC. A durotomy was performed using fine forceps. The prism assembly was lowered into place and secured with Vetbond and black dental cement. A custom head post was affixed to the skull using black dental cement. Prisms were fabricated by cutting 3 mm–by–3 mm coverslips (Warner Instruments, catalog no. 64-0728) to approximately 3 mm–by–2 mm size using a diamond tipped etcher. Coverslips were cleaned with ethanol, dried, and glued onto the brain-facing surface and aluminum-coated hypotenuse of a 2-mm microprism (Tower Optical, catalog no. MPCH-2.0) using ultraviolet curable glue (Norland, catalog no. NOA-61). Mice were given carprofen (5 mg/kg) daily for 5 days after the surgery and allowed to recover for at least 1 week before beginning water restriction and behavioral and imaging studies.

Injection of chABC for slice electrophysiology

Wild-type mice at age P54 to P56 were anesthetized with the ketamine/xylazine cocktail described above. Bupivacaine (2.5 mg/ml, ~0.1 ml) was administered under the scalp for local anesthesia. Craniotomies were made over the left and right GC at the following coordinates: +1.0 mm anterior from bregma and 3.25 mm lateral from midline. A pulled glass pipette was attached to a nanoject pressure injector (Drummond nanjoect II) and filled with chABC in its vehicle (described below). The lipophilic tracer, DiI, was applied to the outside of the glass pipette to later determine the location of chABC injection. The pipette was lowered 2.2 mm below the pia. Approximately 0.25 μl of total volume was injected per side over 10 min. The pipette tip was left in place at least 10 min after the end of the injection. The skin was then suture-closed, and the animal has recovered on a heating pad. Mice were then returned to their home cage, and the LE protocol began 2 days later. Only animals with DiI fluorescence in GC were included in the final analysis (one of the nine mice were removed for missed injection site).

Enzyme infusions

P55 mice were head-restrained, the dummy cannulae were removed, and an injection cannula (33 gauge, 5.0 mm with 0.5-mm projection, Plastics One) was inserted into each guide cannula. Injection cannulae were attached to 10-μl Hamilton syringes via polyethylene tubing from A-M Systems (Sequim, WA). The injection cannulae extended an additional 0.50 mm from the tip of the guide cannulae to reach GC. Bilateral infusions of chABC at 100 U/ml (or Pen at 100 U/ml) were delivered at a flow rate of 0.1 μl/min for a total volume of 0.25 μl per side. Infusion rate was controlled by a pump (Harvard Apparatus). To preserve enzymatic activity, chABC and Pen were dissolved in a vehicle solution containing 50 mM tris-HCl, 60 mM sodium acetate, and 0.2% bovine serum albumin (BSA) (*39*, *54*). Following infusion, the injection cannulae were left in place for 2 min to allow the solution to diffuse from the cannula tips. The dummy cannulae were subsequently reinserted into the guide cannulae. The LE paradigm began 2 days later, on P57.

Two-photon imaging

Imaging experiments began after 4 days of habituation to the behavioral apparatus. Images were acquired on a two-channel movable objective microscope (Sutter) using a resonant scanner controlled by MScan (Sutter) mounted with a 10× super apochromatic objective [Thorlabs, 0.5 numerical aperture, 7.77-mm working distance (WD)]. Fluorophores were excited using a Ti:sapphire femtosecond laser (Coherent) tuned to 980 nm with a laser power of 100 to 250 mW at the front of the objective, and emission was collected using photomultiplier tubes (Hamamatsu). Recording was triggered in episodes ~4 s before the start of each trial. For each episode, 520 frames were acquired at 31 Hz in both the red and green channels. After each session, a 40-μm z stack centered on the imaging plane was obtained for both channels to aid in identification of PV^+ neurons. All mice with sufficient optical window clarity for imaging were trained and included in the analysis.

Electrophysiology

Mice (P34 to P36, P55 to P57, or P90 to P92) were anesthetized with isoflurane using the bell jar method and rapidly decapitated. The brain was dissected in ice-cold, oxygenated standard artificial cerebrospinal fluid (ACSF) containing 126 mM NaCl, 3 mM KCl, 25 mM $NaHCO_3$, 1 mM $NaHPO_4$, 2 mM $MgSO_4$, 2 mM $CaCl_2$, and 14 mM dextrose with an osmolarity of 313 to 317 mosmol with pH 7.4 when bubbled with carbogen (95% oxygen and 5% carbon dioxide). Coronal slices (350 μm) containing GC were prepared using a fresh tissue vibratome (Leica VT1000), allowed to recover in 34°C ACSF for 20 min, and then brought to room temperature (RT) for 30 min before beginning experiments. Individual slices were transferred to the recording chamber and perfused with an ACSF solution optimized to increase spontaneous activity (*38*): 124 mM NaCl, 3.5 mM KCl, 26 mM $NaHCO_3$, 1.25 mM $NaHPO_4$, 0.5 mM $MgCl_2$, 1 mM $CaCl_2$, and 14 mM dextrose, maintained at 34°C with an inline heater (Warner). Whole-cell patch clamp recordings were obtained from visually identified pyramidal neurons under differential interference contrast optics using borosilicate glass pipettes with resistance of 3 to 5 megaohms and filled with a cesium sulfate–based internal solution containing 20 mM KCl, 100 mM Cs-sulfate, 10 mM K-Hepes, 4 mM Mg–adenosine triphosphate (ATP), 0.3 mM Na–guanosine triphosphate (GTP), 10 mM Na-phosphocreatine, 0.2% biocytin (reversal potential (V_{rev})[Cl^{-1}] = −49.3 mV). pH was adjusted to 7.35 with KOH; osmolarity was adjusted to 295 mosmol with sucrose. The sodium channel blocker QX314 (3 mM, Tocris Bioscience) was used to stabilize recordings during prolonged depolarization.

Spontaneous postsynaptic currents were recorded in voltage clamp by holding neurons at three different holding potentials (*75*). For each neuron, current versus holding voltage functions were used to identify the voltage that better isolated the current of interest, which were used for analysis of spontaneous events′ amplitude and frequency (*12*, *38*). To isolate sIPSCs, recordings were obtained around the reversal potential for AMPA- and NMDA-mediated currents (+5, +10, and +15 mV). Cumulative distribution functions were created from 100 sIPSCs from each recorded cell. sEPSCs were recorded at three different holding potentials around the reversal potential for chloride (−55, −50, and −45 mV). Cumulative distribution functions were created from 35 sEPSCs from each recorded cell.

Recordings of input/output functions and analysis of dynamic input resistance (DIR), rheobase, and AP threshold were performed as previously described (*76*) in current clamp with a K-gluconate–based internal solution containing 100 mM K-gluconate, 20 mM KCl, 10 mM K-Hepes, 4 mM Mg-ATP, 0.3 mM Na-GTP, 10 mM Na-phosphocreatine, and 0.4% biocytin; pH was adjusted to 7.35 with KOH; osmolarity was adjusted to 295 mosmol with sucrose. Current steps (700 ms) of increasing intensity (−100 to 400 pA at 50-pA steps) were injected into the cell with a 10-s inter-sweep interval. DIR is reported as the slope of the current-voltage curve for steps below AP threshold. Input/output curves represent the average AP firing frequency for suprathreshold current step for each experimental condition. Rheobase and AP threshold were determined by injecting current steps (700 ms) with increasing intensity (2-pA steps) until the neuron fired one AP for two consecutive sweeps. Rheobase and AP threshold are reported for a subset of neurons in the input/output function analysis, which fired only one AP on at least one current step. Neurons with a series resistance >15 megaohms or that changed >20% during recording were excluded from the analysis. Neuron identity was confirmed post hoc with immunohistochemistry aimed at reconstructing neuron morphology, determining location, and assessing expression of the GABA neuron marker GAD67.

Immunohistochemistry

Validation of cannulae placement or gCaMP7f injection sites

Mice were deeply anesthetized and transcardially perfused with phosphate-buffered saline (PBS), followed by perfusion with 4% paraformaldehyde (PFA) in PBS. Brains were dissected out and postfixed in 4% PFA at 4°C for 3 to 24 hours, followed by cryoprotection in a PBS-buffered sucrose (30%) solution until brains were saturated (~36 hours). Thin (50-μm) coronal brain sections containing the GC were cut on a vibratome (VT1000, Leica). Brain sections were first washed in PBS (three times for 5 min) at RT and then incubated with the nuclear stain, Hoechst 33342 (1:5000, Invitrogen, H3570) in PBST (0.1% Triton X-100) for 30 min at RT. Sections were then washed with PBS (three times for 10 min) and mounted onto glass slides with Fluoromount-G. All sections containing cannulae tracks or gCaMP7f signal were mounted and imaged on a fluorescence microscope (Olympus BX51WI) at ×4 magnification.

PV^+ neuron and PNN labeling

Mice were deeply anesthetized and transcardially perfused with PBS, followed by perfusion with 4% PFA in PBS. Brains were dissected out and postfixed in 4% PFA at 4°C for 3 to 24 hours followed by cryoprotection in a PBS-buffered sucrose (30%) solution until brains were saturated (~36 hours). Thin (50-μm) coronal sections containing GC were cut on a vibratome (VT1000, Leica). Brain sections were first washed in PBS (three times for 5 min) at RT and then blocked in 5% normal goat serum (NGS) and 5% BSA in PBST (0.5% Triton X-100) for 1 hour at RT. These preparatory steps were followed by incubation with primary antibodies overnight at 4°C in a solution containing 2% NGS and 1% BSA in PBST (0.1% Triton X-100). The following antibodies were used for quantification and analysis of fluorescence intensity of PV^+ neurons and PNNs: mouse anti-parvalbumin (1:2000; Swant, PV 235, RRID: AB_10000343) and biotinylated *W. floribunda* lectin (1:500; Vector Laboratories, B-1355-2). Sections were then washed with PBS (three times for 10 min) and incubated with the following fluorescent secondary antibodies at RT for 2 hours: moat anti-mouse

Alexa Fluor 488 (1:200; Thermo Fisher Scientific, A-11029) and streptavidin Alexa Fluor 647 (1:500; Thermo Fisher Scientific, S32357), and counterstained with neuronal-targeting fluorescent Nissl (NeuroTrace 530/615; 1:200; Thermo Fisher Scientific, N21482). After washing with PBS (three times for 10 min), sections were mounted onto glass slides with Fluoromount-G (Southern Biotech). Images were obtained with a laser scanning confocal microscope (Olympus Fluoview) at ×10 magnification. For results presented in Fig. 5 and fig. S7, fluorescence signal quantification was performed on two sections of GC spaced at 150 μm from each animal. The GC outline was previously created and aligned for each section using only the NeuroTrace counterstain to avoid potential bias that might emerge in the PV and WFA signal. Quantification of the number of PV^+ neurons and PNNs as well as of fluorescence intensity was obtained in ImageJ using the Pipsqueak AI macro from Rewire Neuro Inc. (*77*). Individual regions of interest (ROIs) for each PV^+ neuron or PNN were automatically created and verified by an experimenter who was blinded to the experimental condition. All single- or double-labeled neurons or PNNs were detected and analyzed. The proportion of PV^+ neurons associated with PNNs and the intensity of each ROI were also assessed. The proportion of PV^+ neurons was quantified relative to the neuron-specific Nissl-labeled counterstain (NeuroTrace). Quantification of NeuroTrace-positive cells was performed using the ImageJ plugin image–based tool for counting nuclei (Center for Bio-Image Informatics, University of California, Santa Barbara). For validation of chABC-dependent degradation of PNNs presented in Fig. 6, B and C, and fig. S10, analyses were only performed on the left hemisphere in which the unilateral cannula was implanted. Procedures were the same as above, except that quantification was done on three consecutive sections spaced at 50 μm to maximize representation near the tip of the cannulae. For quantification in the piriform cortex, the analyzed area was just ventral to the GC in the most dorsal part of the piriform to maximize the chance of observing differences as this would be the area closest to the cannula.

Labeling of recorded neurons

After electrophysiological recordings, slices were postfixed in 4% PFA for at least 1 week. They were then washed in PBS (three times for 5 min) at RT and then were blocked in 5% NGS and 5% BSA in PBST (1.0% Triton X-100) for 2 to 4 hours at RT, followed by incubation with primary antibodies overnight at 4°C in a solution containing 1% NGS and 1% BSA in PBST (0.1% Triton X-100). The following antibodies were used: streptavidin Alexa Fluor 568 conjugate (1:2000; Invitrogen, S11226) and mouse anti-GAD67 (1:500; MilliporeSigma, MAB5406, monoclonal). Sections were then washed with PBS (three times for 10 min) and incubated with the following fluorescent secondary antibodies at RT for 4 hours: goat anti-mouse Alexa Fluor 488 (1:200; Thermo Fisher Scientific, A-11029), and counterstained with a nuclear stain, Hoechst 33342 (1:5000, Invitrogen, H3570). After washing with PBS (three times for 10 min), sections were mounted onto glass slides with Fluoromount-G. Sections were imaged with a laser scanning confocal microscope (Olympus Fluoview) at ×10 magnification to validate the location within the GC and at ×40 magnification to determine possible colocalization with GAD67.

Data analysis and statistics

Two-photon data analysis

Episodes were downsampled from 31 to 6.2 Hz (ImageJ, grouped Z projection) before downstream processing. Rigid motion correction was performed using NormCorre (*29*) and ROIs, and calcium traces and deconvolved activity were extracted using the constrained nonnegative factorization algorithm (*78*). The automatically detected ROIs were manually curated by inspecting traces and ROI shapes. The deconvolved activity, representing putative spikes, was used in all downstream analysis. PV^+ neurons were identified using the 40-μm z stack obtained at the end of each imaging session. The channels (green and red) were separated, and each stack was collapsed (ImageJ, Z projection). The extracted gCaMP ROIs were overlaid onto the green channel and shifted if necessary to account for potential drift across the motion correction/session. ROIs were then overlaid onto the red (PV) channel, and a 4-pixel annulus was drawn around each ROI (ImageJ, make band). The ratio of the pixel intensity within the ROI to that within the band was computed, and ROIs were sorted on the basis of this ratio (ImageJ, measure). Cells in this sorted list were inspected to determine a cutoff ratio for identifying them as PV^+. All cells above the cutoff value were manually inspected to obtain final PV labels. Cells deemed PV^- were grouped as putative PYR neurons. PV^+ cells consisted of ~5% of imaged cells, consistent with previous studies using cell counting and other approaches (*79*, *80*).

For analysis of baseline activity during the ITI, the mean deconvolved activity across all trials for each neuron was calculated using a 2-s window before trial start (−4 to −2 s before taste delivery). Cumulative distributions of baseline activity for PYR and PV neurons were compared between naïve and EE groups using a two-sample K-S test. Qualitatively similar results were obtained using a longer baseline of 4 s (−6 to −2 s before taste delivery). To identify taste responsive neurons, deconvolved activity was aligned to taste delivery and separated into 1-s bins. A neuron was considered taste responsive if the mean activity in a 1-s baseline before licking onset was significantly different from activity in one of the three bins after taste delivery (rank sum, $P < 0.05$, corrected for six tastes/three bins). Qualitatively similar results were obtained when using a different 1-s baseline. Proportions of responsive neurons were compared using a chi-square test. For curve-fitting analysis, mean activity for each sucrose concentration was identified for each 1-s bin and fit with a linear function. For each fit, 95% CIs were calculated, and a bin was determined to have a significant fit if the CI did not include zero. Neurons were considered to have a significant linear response if at least one bin in the 3-s sampling window displayed a significant fit. For the baseline fit, calculations were performed on an equivalent number of bins, and the proportions of significant fits were compared between naïve and EE using a chi-square test. For the neurons with a significant fit, the absolute maximum slopes were compared in both the baseline and sampling windows using an unpaired two-tailed *t* test.

Brief access test

Analysis of data obtained with the BAT was performed using GraphPad Prism 9, version 9.2.0. A T/W lick ratio was calculated by quantifying the number of licks in each trial and dividing that value by the average licking for all water (0 mM sucrose) trials. Thus, a T/W lick ratio of 1.0 occurred when the licking was similar to licking for water, indicating no difference in preference. Data analysis was done by fitting sigmoid functions to each dataset

with three independent parameters [Top, half maximal inhibitory concentration (IC_{50}), and HillSlope] and one shared parameter (Bottom). Data points and error bars represent means ± SEM. For salt preference curves presented in fig. S3, the sigmoid functions were fit with all four independent parameters (Bottom, Top, IC_{50}, and HillSlope) due to the complex nature of salt preference and avoidance. Sigmoid curves followed the equation

$$Y = \text{Bottom} + (\text{Top} - \text{Bottom}) / \left[1 + \left(\frac{\text{IC}_{50}}{X}\right)^{\text{HillSlope}}\right]$$

Sigmoid fits were plotted as fitted curve ± 95% confidence bands. Fitted curves were analyzed for statistical differences using the extra sum-of-squares F test ("F test"). For BAT experiments involving naïve mice at P56, the same group of 26 naïve mice was used for seven different comparisons across multiple experiments (P56 naïve versus P35 and P91 in Fig. 1B; P56 naïve versus P56 EE in Fig. 1C; P56 naïve versus sucrose-only EE, P56 naïve versus salt only EE, and P56 naïve versus Ensure only EE in Fig. 1D; P56 naïve versus calorie-free EE in Fig. 2A). For these experiments, P value for significance was set to 0.0071 to correct for multiple comparisons.

Lick structure

Analyses were completed using GraphPad Prism 9, version 9.2.0. This analysis was applied both to 30-min water or sucrose sessions (Fig. 1, E and F) and to the 10-s sipper tube availability in the BAT (fig. S6B). Licking bouts were defined as a minimum of three licks, each occurring within 250 ms of the next. Sessions were excluded if the mouse made fewer than 200 licks. Licking bout data were analyzed with Mann-Whitney U test, and accumulated licks were analyzed with two-sample K-S tests. Licks were sorted into bouts using custom Python scripts. Histograms and the Shapiro-Wilks test were conducted to test normality of the data before running post hoc nonparametric statistical tests to compare data. Accumulated licks were calculated using the following equation

$$y = \sum_{i=\text{ILI}(1)}^{\text{ILI}(n)} xi$$

Cumulative distributions

Cumulative distributions of sIPSCs amplitude and frequency were obtained in Igor (WaveMetrics) and Clampfit (Molecular Devices) with the event detection template search. Statistical comparisons were assessed with a two-sample K-S test. To avoid statistical complications of large sample sizes for these datasets (>1000), we applied a more stringent P value of 0.01 for significance. Averages presented represent means ± SEM. Cumulative distributions of fluorescence intensity were extracted from Pipsqueak plugin for ImageJ and analyzed with a two-sample K-S test; intensity averages were analyzed with two-tailed t tests.

Supplementary Materials

This PDF file includes:

Figs. S1 to S10

View/request a protocol for this paper from *Bio-protocol*.

REFERENCES AND NOTES

1. A. Yiannakas, K. Rosenblum, The insula and taste learning. *Front. Mol. Neurosci.* **10**, 335 (2017).
2. J. A. Mennella, C. P. Jagnow, G. K. Beauchamp, Prenatal and postnatal flavor learning by human infants. *Pediatrics* **107**, E88 (2001).
3. K. L. Volcko, D. J. Brakey, J. T. Przybysz, D. Daniels, Exclusively drinking sucrose or saline early in life alters adult drinking behavior by laboratory rats. *Appetite* **149**, 104616 (2020).
4. A. K. Ventura, J. A. Mennella, Innate and learned preferences for sweet taste during childhood. *Curr. Opin. Clin. Nutr. Metab. Care* **14**, 379–384 (2011).
5. A. Fontanini, D. B. Katz, State-dependent modulation of time-varying gustatory responses. *J. Neurophysiol.* **96**, 3183–3193 (2006).
6. D. B. Katz, S. A. Simon, M. A. Nicolelis, Dynamic and multimodal responses of gustatory cortical neurons in awake rats. *J. Neurosci.* **21**, 4478–4489 (2001).
7. M. G. Veldhuizen, D. Douglas, K. Aschenbrenner, D. R. Gitelman, D. M. Small, The anterior insular cortex represents breaches of taste identity expectation. *J. Neurosci.* **31**, 14735–14744 (2011).
8. Y. Livneh, R. N. Ramesh, C. R. Burgess, K. M. Levandowski, J. C. Madara, H. Fenselau, G. J. Goldey, V. E. Diaz, N. Jikomes, J. M. Resch, B. B. Lowell, M. L. Andermann, Homeostatic circuits selectively gate food cue responses in insular cortex. *Nature* **546**, 611–616 (2017).
9. C. L. Samuelsen, M. P. Gardner, A. Fontanini, Effects of cue-triggered expectation on cortical processing of taste. *Neuron* **74**, 410–422 (2012).
10. M. P. Gardner, A. Fontanini, Encoding and tracking of outcome-specific expectancy in the gustatory cortex of alert rats. *J. Neurosci.* **34**, 13000–13017 (2014).
11. D. E. Berman, Y. Dudai, Memory extinction, learning anew, and learning the new: Dissociations in the molecular machinery of learning in cortex. *Science* **291**, 2417–2419 (2001).
12. M. S. Haley, A. Fontanini, A. Maffei, Laminar- and target-specific amygdalar inputs in rat primary gustatory cortex. *J. Neurosci.* **36**, 2623–2637 (2016).
13. I. E. de Araujo, A. J. Oliveira-Maia, T. D. Sotnikova, R. R. Gainetdinov, M. G. Caron, M. A. Nicolelis, S. A. Simon, Food reward in the absence of taste receptor signaling. *Neuron* **57**, 930–941 (2008).
14. H. C. Schiff, A. L. Bouhuis, K. Yu, M. A. Penzo, H. Li, M. He, B. Li, An insula-central amygdala circuit for guiding tastant-reinforced choice behavior. *J. Neurosci.* **38**, 1418–1429 (2018).
15. R. Vincis, K. Chen, L. Czarnecki, J. Chen, A. Fontanini, Dynamic representation of taste-related decisions in the gustatory Insular cortex of mice. *Curr. Biol.* **30**, 1834–1844.e5 (2020).
16. C. E. May, A. Vaziri, Y. Q. Lin, O. Grushko, M. Khabiri, Q. P. Wang, K. J. Holme, S. D. Pletcher, P. L. Freddolino, G. G. Neely, M. Dus, High dietary sugar reshapes sweet taste to promote feeding behavior in Drosophila melanogaster. *Cell Rep.* **27**, 1675–1685.e7 (2019).
17. J. C. Smith, The history of the "Davis Rig". *Appetite* **36**, 93–98 (2001).
18. C. Inui-Yamamoto, T. Yamamoto, K. Ueda, M. Nakatsuka, S. Kumabe, T. Inui, Y. Iwai, Taste preference changes throughout different life stages in male rats. *PLOS ONE* **12**, e0181650 (2017).
19. J. J. Wurtman, R. J. Wurtman, Sucrose consumption early in life fails to modify the appetite of adult rats for sweet foods. *Science* **205**, 321–322 (1979).
20. M. Smriga, M. Kameishi, K. Torii, Brief exposure to NaCl during early postnatal development enhances adult intake of sweet and salty compounds. *Neuroreport* **13**, 2565–2569 (2002).
21. A. C. Spector, P. A. Klumpp, J. M. Kaplan, Analytical issues in the evaluation of food deprivation and sucrose concentration effects on the microstructure of licking behavior in the rat. *Behav. Neurosci.* **112**, 678–694 (1998).
22. J. D. Davis, G. P. Smith, B. Singh, A microstructural analysis of the control of water and isotonic saline ingestion by postingestional stimulation. *Physiol. Behav.* **66**, 543–548 (1999).
23. J. K. Roebber, S. Izenwasser, N. Chaudhari, Cocaine decreases saccharin preference without altering sweet taste sensitivity. *Pharmacol. Biochem. Behav.* **133**, 18–24 (2015).
24. B. M. Slotnick, L. A. Gutman, Evaluation of intranasal zinc sulfate treatment on olfactory discrimination in rats. *J. Comp. Physiol. Psychol.* **91**, 942–950 (1977).
25. I. Kusumoto-Yoshida, H. Liu, B. T. Chen, A. Fontanini, A. Bonci, Central role for the insular cortex in mediating conditioned responses to anticipatory cues. *Proc. Natl. Acad. Sci. U.S.A.* **112**, 1190–1195 (2015).
26. R. Vincis, A. Fontanini, Associative learning changes cross-modal representations in the gustatory cortex. *eLife* **5**, e16420 (2016).
27. H. Taniguchi, M. He, P. Wu, S. Kim, R. Paik, K. Sugino, D. Kvitsiani, Y. Fu, J. Lu, Y. Lin, G. Miyoshi, Y. Shima, G. Fishell, S. B. Nelson, Z. J. Huang, A resource of Cre driver lines for genetic targeting of GABAergic neurons in cerebral cortex. *Neuron* **71**, 995–1013 (2011).
28. L. Madisen, T. A. Zwingman, S. M. Sunkin, S. W. Oh, H. A. Zariwala, H. Gu, L. L. Ng, R. D. Palmiter, M. J. Hawrylycz, A. R. Jones, E. S. Lein, H. Zeng, A robust and high-throughput Cre reporting and characterization system for the whole mouse brain. *Nat. Neurosci.* **13**, 133–140 (2010).

29. E. A. Pnevmatikakis, A. Giovannucci, NoRMCorre: An online algorithm for piecewise rigid motion correction of calcium imaging data. *J. Neurosci. Methods* **291**, 83–94 (2017).
30. G. Di Cristo, B. Chattopadhyaya, S. J. Kuhlman, Y. Fu, M. C. Belanger, C. Z. Wu, U. Rutishauser, L. Maffei, Z. J. Huang, Activity-dependent PSA expression regulates inhibitory maturation and onset of critical period plasticity. *Nat. Neurosci.* **10**, 1569–1577 (2007).
31. D. D. Rupert, S. D. Shea, Parvalbumin-positive interneurons regulate cortical sensory plasticity in adulthood and development through shared mechanisms. *Front. Neural. Circuits* **16**, 886629 (2022).
32. A. Yiannakas, S. Kolatt Chandran, H. Kayyal, N. Gould, M. Khamaisy, K. Rosenblum, Parvalbumin interneuron inhibition onto anterior insula neurons projecting to the basolateral amygdala drives aversive taste memory retrieval. *Curr. Biol.* **31**, 2770–2784.e6 (2021).
33. N. Berardi, T. Pizzorusso, L. Maffei, Extracellular matrix and visual cortical plasticity: Freeing the synapse. *Neuron* **44**, 905–908 (2004).
34. T. Pizzorusso, P. Medini, N. Berardi, S. Chierzi, J. W. Fawcett, L. Maffei, Reactivation of ocular dominance plasticity in the adult visual cortex. *Science* **298**, 1248–1251 (2002).
35. B. A. Sorg, S. Berretta, J. M. Blacktop, J. W. Fawcett, H. Kitagawa, J. C. Kwok, M. Miquel, Casting a wide net: Role of perineuronal nets in neural plasticity. *J. Neurosci.* **36**, 11459–11468 (2016).
36. S. Murase, C. L. Lantz, E. M. Quinlan, Light reintroduction after dark exposure reactivates plasticity in adults via perisynaptic activation of MMP-9. *eLife* **6**, e27345 (2017).
37. F. Donato, S. B. Rompani, P. Caroni, Parvalbumin-expressing basket-cell network plasticity induced by experience regulates adult learning. *Nature* **504**, 272–276 (2013).
38. L. A. Schier, K. M. Hyde, A. C. Spector, Conditioned taste aversion versus avoidance: A re-examination of the separate processes hypothesis. *PLoS One* **14**, e0217458 (2019).
39. E. Favuzzi, A. Marques-Smith, R. Deogracias, C. M. Winterflood, A. Sanchez-Aguilera, L. Mantoan, P. Maeso, C. Fernandes, H. Ewers, B. Rico, Activity-dependent gating of parvalbumin interneuron function by the perineuronal net protein brevican. *Neuron* **95**, 639–655.e10 (2017).
40. R. Lin, J. C. Kwok, D. Crespo, J. W. Fawcett, Chondroitinase ABC has a long-lasting effect on chondroitin sulphate glycosaminoglycan content in the injured rat brain. *J. Neurochem.* **104**, 400–408 (2008).
41. J. X. Maier, Single-neuron responses to intraoral delivery of odor solutions in primary olfactory and gustatory cortex. *J. Neurophysiol.* **117**, 1293–1304 (2017).
42. C. L. Samuelsen, A. Fontanini, Processing of intraoral olfactory and gustatory signals in the gustatory cortex of awake rats. *J. Neurosci.* **37**, 244–257 (2017).
43. J. X. Maier, M. Wachowiak, D. B. Katz, Chemosensory convergence on primary olfactory cortex. *J. Neurosci.* **32**, 17037–17047 (2012).
44. M. L. Blankenship, M. Grigorova, D. B. Katz, J. X. Maier, Retronasal odor perception requires taste cortex, but orthonasal does not. *Curr. Biol.* **29**, 62–69.e3 (2019).
45. N. Gogolla, A. E. Takesian, G. Feng, M. Fagiolini, T. K. Hensch, Sensory integration in mouse insular cortex reflects GABA circuit maturation. *Neuron* **83**, 894–905 (2014).
46. T. K. Hensch, Critical period regulation. *Annu. Rev. Neurosci.* **27**, 549–579 (2004).
47. M. S. Haley, S. Bruno, A. Fontanini, A. Maffei, LTD at amygdalocortical synapses as a novel mechanism for hedonic learning. *eLife* **9**, e55175 (2020).
48. A. Vaziri, M. Khabiri, B. T. Genaw, C. E. May, P. L. Freddolino, M. Dus, Persistent epigenetic reprogramming of sweet taste by diet. *Sci. Adv.* **6**, eabc8492 (2020).
49. D. L. Hill, R. M. Bradley, C. M. Mistretta, Development of taste responses in rat nucleus of solitary tract. *J. Neurophysiol.* **50**, 879–895 (1983).
50. C. Sun, E. Hummler, D. L. Hill, Selective deletion of sodium salt taste during development leads to expanded terminal fields of gustatory nerves in the adult mouse nucleus of the solitary tract. *J. Neurosci.* **37**, 660–672 (2017).
51. K. Touzani, A. Sclafani, Insular cortex lesions fail to block flavor and taste preference learning in rats. *Eur. J. Neurosci.* **26**, 1692–1700 (2007).
52. M. B. Bales, L. A. Schier, G. D. Blonde, A. C. Spector, Extensive gustatory cortex lesions significantly impair taste sensitivity to KCl and quinine but not to sucrose in rats. *PLOS ONE* **10**, e0143419 (2015).
53. M. B. Bales, A. C. Spector, Chemospecific deficits in taste sensitivity following bilateral or right hemispheric gustatory cortex lesions in rats. *J. Comp. Neurol.* **528**, 2729–2747 (2020).
54. T. Pizzorusso, P. Medini, S. Landi, S. Baldini, N. Berardi, L. Maffei, Structural and functional recovery from early monocular deprivation in adult rats. *Proc. Natl. Acad. Sci. U.S.A.* **103**, 8517–8522 (2006).
55. Y. Hada, Y. Yamada, K. Imamura, N. Mataga, Y. Watanabe, M. Yamamoto, Effects of monocular enucleation on parvalbumin in rat visual system during postnatal development. *Invest. Ophthalmol. Vis. Sci.* **40**, 2535–2545 (1999).
56. F. Donato, A. Chowdhury, M. Lahr, P. Caroni, Early- and late-born parvalbumin basket cell subpopulations exhibiting distinct regulation and roles in learning. *Neuron* **85**, 770–786 (2015).
57. S. Mellado, B. Moreno-Ruiz, S. Exposito, M. Fernandez, E. D. Martin, Prolactin reduces hippocampal parvalbumin and GABAA receptor expression in female mice. *Neuroendocrinology* **112**, 796–806 (2022).
58. L. S. Callahan, K. A. Thibert, J. D. Wobken, M. K. Georgieff, Early-life iron deficiency anemia alters the development and long-term expression of parvalbumin and perineuronal nets in the rat hippocampus. *Dev. Neurosci.* **35**, 427–436 (2013).
59. L. Alberi, A. Lintas, R. Kretz, B. Schwaller, A. E. Villa, The calcium-binding protein parvalbumin modulates the firing 1 properties of the reticular thalamic nucleus bursting neurons. *J. Neurophysiol.* **109**, 2827–2841 (2013).
60. R. Tremblay, S. Lee, B. Rudy, GABAergic interneurons in the neocortex: From cellular properties to circuits. *Neuron* **91**, 260–292 (2016).
61. B. Chattopadhyaya, G. Di Cristo, H. Higashiyama, G. W. Knott, S. J. Kuhlman, E. Welker, Z. J. Huang, Experience and activity-dependent maturation of perisomatic GABAergic innervation in primary visual cortex during a postnatal critical period. *J. Neurosci.* **24**, 9598–9611 (2004).
62. A. Maffei, K. Nataraj, S. B. Nelson, G. G. Turrigiano, Potentiation of cortical inhibition by visual deprivation. *Nature* **443**, 81–84 (2006).
63. L. Wang, A. Maffei, Inhibitory plasticity dictates the sign of plasticity at excitatory synapses. *J. Neurosci.* **34**, 1083–1093 (2014).
64. F. Beker, H. G. Liley, I. P. Hughes, S. E. Jacobs, J. Macey, E. Twitchell, P. G. Davis, Effects on growth of smell and taste of milk during tube feeding of preterm infants: A randomized clinical trial. *JAMA Pediatr.* **175**, 1115–1123 (2021).
65. B. Smith, S. L. Rogers, J. Blissett, A. K. Ludlow, The relationship between sensory sensitivity, food fussiness and food preferences in children with neurodevelopmental disorders. *Appetite* **150**, 104643 (2020).
66. N. Chen, K. Watanabe, T. Kobayakawa, M. Wada, Relationships between autistic traits, taste preference, taste perception, and eating behaviour. *Eur. Eat. Disord. Rev.* **30**, 628–640 (2022).
67. L. T. Chistol, L. G. Bandini, A. Must, S. Phillips, S. A. Cermak, C. Curtin, Sensory sensitivity and food selectivity in children with autism spectrum disorder. *J. Autism Dev. Disord.* **48**, 583–591 (2018).
68. J. F. Cryan, T. G. Dinan, Mind-altering microorganisms: The impact of the gut microbiota on brain and behaviour. *Nat. Rev. Neurosci.* **13**, 701–712 (2012).
69. E. Barrett, R. P. Ross, P. W. O'Toole, G. F. Fitzgerald, C. Stanton, gamma-Aminobutyric acid production by culturable bacteria from the human intestine. *J. Appl. Microbiol.* **113**, 411–417 (2012).
70. L. A. Czarnecki, A. H. Moberly, T. Rubinstein, D. J. Turkel, J. Pottackal, J. P. McGann, In vivo visualization of olfactory pathophysiology induced by intranasal cadmium instillation in mice. *Neurotoxicology* **32**, 441–449 (2011).
71. J. I. Glendinning, J. Gresack, A. C. Spector, A high-throughput screening procedure for identifying mice with aberrant taste and oromotor function. *Chem. Senses* **27**, 461–474 (2002).
72. B. Slotnick, A simple 2-transistor touch or lick detector circuit. *J. Exp. Anal. Behav.* **91**, 253–255 (2009).
73. M. Yang, J. N. Crawley, Simple behavioral assessment of mouse olfaction. *Curr. Protoc. Neurosci.* **Chapter 8**, Unit 8.24 (2009).
74. M. D. Kass, A. H. Moberly, J. P. McGann, Spatiotemporal alterations in primary odorant representations in olfactory marker protein knockout mice. *PLoS One* **8**, e61431 (2013).
75. R. Tatti, O. K. Swanson, M. S. E. Lee, A. Maffei, Layer-specific developmental changes in excitation and inhibition in rat primary visual cortex. *eNeuro* **4**, ENEURO.0402-17.2017 (2017).
76. O. K. Swanson, R. Semaan, A. Maffei, Reduced dopamine signaling impacts pyramidal neuron excitability in mouse motor cortex. *eNeuro* **8**, ENEURO.0548-19.2021 (2021).
77. M. L. Slaker, J. H. Harkness, B. A. Sorg, A standardized and automated method of perineuronal net analysis using Wisteria floribunda agglutinin staining intensity. *IBRO Rep.* **1**, 54–60 (2016).
78. E. A. Pnevmatikakis, D. Soudry, Y. Gao, T. A. Machado, J. Merel, D. Pfau, T. Reardon, Y. Mu, C. Lacefield, W. Yang, M. Ahrens, R. Bruno, T. M. Jessell, D. S. Peterka, R. Yuste, L. Paninski, Simultaneous denoising, deconvolution, and demixing of calcium imaging data. *Neuron* **89**, 285–299 (2016).
79. Y. Gonchar, Q. Wang, A. Burkhalter, Multiple distinct subtypes of GABAergic neurons in mouse visual cortex identified by triple immunostaining. *Front Neuroanat* **1**, 3 (2007).
80. Y. Kim, G. R. Yang, K. Pradhan, K. U. Venkataraju, M. Bota, L. C. García Del Molino, G. Fitzgerald, K. Ram, M. He, J. M. Levine, P. Mitra, Z. J. Huang, X. J. Wang, P. Osten, Brain-wide Maps reveal stereotyped cell-type-based cortical architecture and subcortical sexual dimorphism. *Cell* **171**, 456–469.e22 (2017).

Acknowledgments
Funding: This work was supported by National Institutes of Health grants R01DC019827 to A.M., R01DC013770 to A.M. and A.F., R01DC015234 to A.F. and A.M., and UF1NS115779 to A.F. and A.M.; and National Institutes of Health Fellowship F32DC018485 to H.C.S. and F30DC019523 to J.F.K. **Author contributions:** Designed experiments: H.C.S., J.F.K., M.I., L.A.C., A.F., and A.M. Performed experiments: H.C.S., J.F.K., M.I., and L.A.C. Analyzed data: H.C.S., J.F.K., M.I., and L.A.C. Supervised experiments and analysis: A.F. and A.M. Writing: H.C.S., J.F.K., M.I., L.A.C., A.F., and A.M. **Competing interests:** The authors declare that they have no competing interests. **Data and materials availability:** All data needed to evaluate the conclusions in the paper are present in the paper and/or the Supplementary Materials.

Submitted 30 August 2022
Accepted 7 December 2022
Published 11 January 2023
10.1126/sciadv.ade6561